Progress in Surface Science 87 (2012) 163–188

Contents lists available at SciVerse ScienceDirect

Progress in Surface Science

journal homepage: www.elsevier.com/locate/progsurf

Review

Stages of hot electron dynamics in multiexcitation processes at surfaces: General properties and benchmark examples

Branko Gumhalter

Institute of Physics, HR-10000 Zagreb, Croatia

ARTICLE INFO

Keywords:
Hot electron dynamics
Surface bands
Ultrafast spectroscopies
Multiexcitation processes
non-Markovian quasiparticle dynamics
Transient surface response

ABSTRACT

Ultrafast spectroscopy studies of the electronic properties of surfaces and nanostructures have greatly advanced our knowledge of nonequilibrium electron dynamics in the systems with reduced dimensionality. Underlying to the understanding of ultrafast phenomena on surfaces of solids is the problem of hot electron (hole) dynamics and decoherence in unoccupied (occupied) bands. The need for deeper insight into these phenomena has revived the interest in many-body interactions of quasiparticles with the dynamical degrees of freedom which constitute bosonic heatbath of the system. Simple descriptions of these processes in terms of quasiparticle propagators are hindered by the failure of traditional approximations to reproduce equally reliably the quasiparticle spectral properties in the entire range from the excitation threshold to higher multiexcitation energies. To remedy this situation and enable the description of quasiparticle dynamics throughout the pertinent bands we develop a unified approach for construction of propagators in the time-domain which is based on the mapping of standard quasiparticle spectral representation to the cumulant form. We combine the features of low order cumulant expansion, which accurately describes multiple excitation processes in the preasymptotic regime, with cumulant mapping of perturbation theory results from the band bottom to account for the asymptotic quasiparticle decay. Thereby we obtain a complete representation of the various temporal stages of propagation of band electrons (or holes) coupled to the system heatbath. The described procedure is illustrated with examples of nonadiabatic quasiparticle dynamics in benchmark systems of increasing complexity. The sequence is concluded with the analysis of amplitude and phase transients and decoherence phenomena leading to deviations from Markovian dynamics of quasiparticles in the

E-mail address: branko@ifs.hr

0079-6816/$ - see front matter
http://dx.doi.org/10.1016/j.progsurf.2012.05.004

paradigmatic quasi-two dimensional image potential bands on Cu (1 1 1) surface. Lastly, we outline the spectroscopic investigations of surfaces in which manifestations of these effects should be recognized in the interpretations of measurements.

Contents

1. Introduction

1.1. Rationale for time-domain approach to quasiparticle dynamics at surfaces

Spectroscopic studies of bulk and surface electronic structure of solids provide valuable information on the properties of electronic states generated by the interactions of electrons with atomic structure and intrinsic degrees of freedom of the probed system. For complex and large systems the deconvolutions of one-electron features from the measured spectra are difficult, particularly in the experiments involving strongly excited intermediate and final states accommodating hot quasiparticles (electrons and holes). In this case it is usually more convenient and insightful to resort to time domain descriptions of experimental results [1]. The situation becomes additionally complicated in time-resolved measurements using ultrafast probes which *per se* introduce specific features into the already complex temporal evolution of excited quasiparticles and the system as a whole. Understanding of these processes requires good modelling of nonstationary quasiparticle dynamics within the many-body framework because nonadiabatic phenomena can strongly influence the results of ultrafast measurements.

Effects associated with nonadiabatic quasiparticle dynamics are expected to manifest themselves most clearly in combined state- and time-resolved measurements. At present the prime experimental tools for providing new insights into dynamical processes at surfaces are ultrafast pump–probe spectroscopies with high temporal resolution [2]. In this context the two-photon photoemission [3–6] (2PPE) and multi-photon photoemission [7,8] (MPPE) spectroscopy utilizing ultrashort excitation pulses enable tracing the evolution of hot quasiparticles from their preparation in the primary

excited state, over the period of early transients and steady state decay to the asymptotic regime of quasiparticle collapse or thermalization. The present work is devoted to the development of a unified quantum–mechanical model for time-domain description of these phenomena and their manifestations in the quasiparticle propagators and correlation functions directly related to physical observables that are accessible in linear and nonlinear spectroscopies of atoms, solids and molecular aggregates [1,4–6,9–16]. Using the present approach we are able to generalize and complement the earlier treatments of ultrafast quasiparticle dynamics in surface bands [17–21] by extending them over the entire intervals of observation currently attainable in time-resolved experiments.

1.2. Quasiparticles in interaction with the heatbath

Primary excitation processes in pump–probe photoemission spectroscopy of surfaces are the pump induced electronic transitions from occupied states to unoccupied surface localized states or bands lying between the vacuum level E_V and the Fermi energy E_F of the system. In 2PPE and MPPE the characteristics of these intermediate states are explored by the probe pulse which lifts the excited electrons to final outgoing states in which they are detected. Propagation of hot electrons (holes) created in empty (occupied) states at surfaces is subject to the interactions with excitations of the system heatbath. This affects the dynamics of quasiparticles in the intermediate states and thereby also the characteristics of the final photoelectron signal. For moderate and strong coupling strength such interactions may add complex features to the photoemitted electron spectra and their interpretation requires good modelling of the underlying intermediate state quasiparticle dynamics. On the general level the problem has a long history [22] which can be optimally exploited. For decades one of the central issues in many-body theory has been a realistic description of multiple excitation processes arising from quasiparticle coupling to dynamical degrees of freedom of the environment. A simple paradigmatic but highly relevant theoretical description of these phenomena is provided by a model of single particle in interaction with bosonic excitations constituting the heatbath. These may represent a variety of vibrational, charge or spin density and other bosonized excitations in the system, and hence a large class of dynamical processes encountered in the studies of condensed matter systems can be mapped onto this model [22–24].

Despite the seeming simplicity of the particle–boson model, its application to the studies of dynamics of quasiparticles in strong interaction with the heatbath excitations poses considerable difficulties. The major one arises in the calculations of propagators and their spectral properties used for description of quasiparticle dynamics in highly excited intermediate states. The calculations based on standard perturbative schemes prove inadequate if restricted to the weak excitation limit and mainly intractable beyond it. In particular, applications of the various forms of popular GW-approximation [25–29] (GWA) to calculations of the effects of particle–boson interactions on the quasiparticle spectra produce only the singly excited satellite structure above the quasielastic peak. Moreover, GWA fails to predict the correct energy and weight of the inelastic component of the spectrum [28–31] in comparison with the results of alternative approaches [30–40] or exactly solvable models [22,41–45]. Analogous trends have been observed in the applications of GWA to other many-body problems [46]. Several nonperturbative approaches to calculating the spectra of particles coupled to boson fields have been developed following the analogies with exact solutions of simple models [22,41–43]. In the focus of these approaches was a correct description of the satellite spectral structures arising from multiple boson excitations but less attention has been paid to the descriptions of nonadiabatic processes leading to quasiparticle decoherence and decay throughout the entire propagation interval. However, recent temporally resolved optical experiments have demonstrated some hitherto undetected peculiar features of particle dynamics in quantum systems [47,48] which call for careful examination of the decoherence phenomena.

To establish the required unified description of hot electron and hole dynamics in the systems of reduced dimensionality we start in Section 2 from a general particle–boson model and use it for the definition of cumulant representation of quasiparticle propagators in the real time domain. In Section 3 we construct and discuss the solutions of the model which satisfy the temporal boundary conditions of ultrafast experiments. We illustrate on a series of examples the various manifestations of nonadiabatic quasiparticle dynamics and transient phenomena that may be triggered by ultrafast per-

turbations. In Section 4 we elaborate the applications of this approach to electron or hole propagation in quasi-two dimensional (Q2D) surface bands and illustrate the salient characteristics of obtained solutions in the case of paradigmatic image potential bands on Cu (1 1 1) surface. In Section 5 we discuss the non-Markovian features of quasiparticle decoherence and decay predicted by the developed model and outline experimental conditions and regimes in which their effect on the measured spectra may be expected and detected.

2. Representation of single particle propagator in exponential form

Interpretation of the final measured signal of 2PPE and MPPE requires the knowledge of both the adiabatic and nonadiabatic aspects of hot quasiparticle dynamics in the initial (hole) and the intermediate states (electron) of the excitation pathways. This information can be retrieved from the quasiparticle propagators. In the following we shall restrict our considerations to modelling of hot electron dynamics in empty bands characteristic of the intermediate states in 2PPE and MPPE, as well as the final states in inverse photoemission from solids. The description of hole dynamics in occupied bands, which is needed equally in the descriptions of MPPE, 2PPE [15,49] and one-photon photoemission spectra from solids [9–13], can then be obtained by time reversal.

The dynamics of an electron excited (promoted) into an empty band is in the absence of interactions leading to incoherent processes described by the effective one-particle (superscript p) Hamiltonian:

$$H_0^p = \sum_{\mathbf{k}} \epsilon_{\mathbf{k}} c_{\mathbf{k}}^\dagger c_{\mathbf{k}}. \tag{1}$$

Here the quantum number $\mathbf{k}$ is short for the particle (quasi) momentum and band index, $\epsilon_{\mathbf{k}}$ is the energy dispersion within the band, and $c_{\mathbf{k}}^\dagger$ and $c_{\mathbf{k}}$ denote the electron creation and annihilation operators in the state $|\mathbf{k}\rangle$, respectively. The unperturbed band bottom is identified with the minimum value(s) of $\epsilon_{\mathbf{k}}$. The one particle eigenstates $|\mathbf{k}\rangle$ of H_0^p constitute a convenient basis set for the description of the effects of various perturbations on the quasiparticle motion within the band. The interaction of the excited electron with the dynamical degrees of freedom of the heatbath is modelled by a coupling to bosonic excitations. The Hamiltonian of unperturbed bosons (superscript b) is given by

$$H_0^b = \sum_{\mathbf{q}} \omega_{\mathbf{q}} a_{\mathbf{q}}^\dagger a_{\mathbf{q}}, \tag{2}$$

where $a_{\mathbf{q}}$ and $a_{\mathbf{q}}^\dagger$ denote the annihilation and creation operators, respectively, for boson excitations characterized by the (quasi) momentum $\mathbf{q}$ and energy $\omega_{\mathbf{q}}$. A typical example of interactions of particles with a heatbath is rendered by the linear coupling to vibrational or bosonized electronic degrees of freedom in the solid which was shown to play the dominant role in the energy and momentum exchange between the two subsystems [50]. In this archetype case the interaction takes the form

$$V = \sum_{\mathbf{k}',\mathbf{k},\mathbf{q}} V_{\mathbf{k}',\mathbf{k}}^{\mathbf{q}} c_{\mathbf{k}'}^\dagger c_{\mathbf{k}} \left(a_{\mathbf{q}} + a_{-\mathbf{q}}^\dagger \right). \tag{3}$$

In the present single-particle problem the interaction V is nonvanishing only after the particle introduction into the band.

Prior to electron injection into the empty band the system is in its ground state $|0\rangle$ which is an eigenstate of $H_0 = H_0^p + H_0^b$ with the energy E_0 and all the band and boson states empty. After the electron promotion into an eigenstate $|\mathbf{k}\rangle = c_{\mathbf{k}}^\dagger |0\rangle$ of H_0 its dynamics is governed by the full Hamiltonian

$$H = H_0^p + H_0^b + V = H_0 + V. \tag{4}$$

The evolution of the initial electron state $|\mathbf{k}\rangle$ is most conveniently studied by exploring the properties of retarded $\mathbf{k}$-diagonal quasiparticle propagator [51]

$$\begin{aligned} G_{\mathbf{k}}(t) &= -i\theta(t)\langle 0|c_{\mathbf{k}}(t)c_{\mathbf{k}}^\dagger(0)|0\rangle = -i\theta(t)e^{iE_0 t}\langle 0|c_{\mathbf{k}}e^{-iHt}c_{\mathbf{k}}^\dagger|0\rangle = -i\theta(t)e^{-i\epsilon_{\mathbf{k}}t}\langle \mathbf{k}|U_I(t)|\mathbf{k}\rangle \\ &= G_{\mathbf{k}}^0(t)e^{C(\mathbf{k},t)}. \end{aligned} \tag{5}$$

Here t is the propagation time subsequent to quasiparticle creation in the initial band state $|\mathbf{k}\rangle$, $H|0\rangle = H_0|0\rangle = E_0|0\rangle$, $U_I(t)$ is the evolution operator in the interaction picture, and $G^0_{\mathbf{k}}(t) = -i\theta(t)e^{-i\epsilon_{\mathbf{k}}t}$ denotes the unperturbed single particle propagator where $\theta(t)$ is the Heaviside step function. The cumulant function

$$C(\mathbf{k},t) = \sum_{n=2}^{\infty} C_n(\mathbf{k},t) \tag{6}$$

sometimes also called the lineshape generator, appears as a sum of all cumulants [52] generated by the interaction V in the basis of eigenstates of H_0. For the interaction (3) the first nonvanishing cumulant is quadratic in $V^{\mathbf{q}}_{\mathbf{k}',\mathbf{k}}$.

Cumulant representation of the single particle propagator (5) is exact [52] but the calculations of higher order terms C_n in (6) for $n > 4$ usually pose unsurmountable difficulties [17,37,43,53–55]. However, since the cumulant series (6) is an expansion in the strengths of irreducible phase space correlations between subsequent scattering events [52] (i.e. not only in the powers of the coupling constant), the convergence of the series is very fast provided such correlations are weak. This proves to be the case in cascade processes of successive one-boson emissions and absorptions. In these situations only the lowest order cumulants are relevant and a very small error is incurred by terminating the series already after the first nonvanishing term C_2 or the lowest two terms $C_2 + C_4$ [17].

The advantage of representing the quasiparticle propagator in the form given by the last line of expression (5) is usually illustrated in the extremely simple but physically relevant limit of the particle band reduced to a single orbital state in interaction with the field of nondispersive bosons. In this case the problem is exactly soluble by the second order cumulant $C_2(t)$ and the resulting quasiparticle spectrum appears as an infinite series of equally separated delta-function peaks weighted by the Poisson distribution [22,41] (cf. Section 3.2 below). Another related and exactly soluble problem is the so-called forced oscillator model (FOM) in which the action of the quasiparticle on displacements of the boson field is represented by a classical time-dependent perturbation [56,57]. Here it is important to reiterate that in both examples the exact solution is provided by $C_2(t)$ which does not contain correlations between successive multiexcitation processes. In the treatment of more complicated models describing interactions of band electrons with optical phonons and with bosonized charge density fluctuations in solids explicit expressions for the second and fourth order cumulants were derived in Refs. [54,17], respectively. These works demonstrated that for realistic coupling strengths the major contribution to cumulant series comes from the second order term. This property of lowest order cumulants was exploited to study non-Markovian quasiparticle propagation in surface bands from the early ballistic, over the subsequent transient, to the intermediate stage of exponential decay of electronic states [18,19]. However, the complete description that would include also the long-time asymptotic quasiparticle decay [58] leading to a collapse of the propagator amplitude and phase [15,20,21] remains inaccessible to the lowest order cumulant approach. The following discussion is focused on overcoming this deficiency in applications of the otherwise computationally very convenient and powerful cumulant method.

Quite generally, the retarded single particle propagator $G_{\mathbf{k}}(t)$ can be expressed in the spectral representation [59]

$$G_{\mathbf{k}}(t) = -i\theta(t)\int_{-\infty}^{\infty} \mathcal{N}(\mathbf{k},\omega')e^{-i\omega' t}d\omega'. \tag{7}$$

The quasiparticle spectrum $\mathcal{N}(\mathbf{k},\omega')$ is a fundamental quantity that determines the quasiparticle propagator and its basic properties follow directly from the initial definition of $G_{\mathbf{k}}(t)$. One way to establish the relation between cumulant and standard spectral representation of the propagator (7) is to expand $\exp[\sum_n C_n(\mathbf{k},t)]$ in the power series and equate the obtained terms with the terms of the corresponding self-energy expansion of (7) that are of the same order in the interaction V [22,37,55]. However, this approach encounters several difficulties. The first is awkward form of the higher order terms which inevitably leads to computational problems. Second, handling the terms of such series may be problematic in the cases of decay processes for which $\Re C_n(t) \propto -\Gamma_n t$ or $\Re C_n(t) \propto -\beta_n \ln t$ whose divergences at long times must be carefully dealt with. Hence, in the follow-

ing we adopt a different approach. In analogy with the results of exactly solvable models [41,45] and second order cumulant expansion [17,19,43] we define the ρ-representability of the cumulant sum (6) in the form

$$C(\mathbf{k},t) = -\int_{-\infty}^{\infty} \rho(\mathbf{k},\omega)\frac{1-i\omega t - e^{-i\omega t}}{\omega^2}d\omega \tag{8}$$

which is a Taylor expandable function around $t = 0$. The yet unknown cumulant spectrum

$$\rho(\mathbf{k},\omega) = \sum_{l=2}^{\infty}\rho_l(\mathbf{k},\omega) \tag{9}$$

stands for a sum of the interaction-induced cumulant spectral components in powers of the interaction V. For translationally invariant systems the form of the leading term $\rho_2(\mathbf{k},\omega)$ that yields $C_2(\mathbf{k},t)$ is known from the earlier studies [17,43] and reads:

$$\rho_2(\mathbf{k},\omega) = \sum_{\mathbf{q}}\left|V^{\mathbf{q}}_{\mathbf{k},\mathbf{k}-\mathbf{q}}\right|^2\delta(\omega-\epsilon_{\mathbf{k}-\mathbf{q}}-\omega_{\mathbf{q}}+\epsilon_{\mathbf{k}}). \tag{10}$$

$C(\mathbf{k},t)$ satisfies the unitarity and boundary conditions arising from the properties of the evolution operator generated by V. Hence

$$C^*(\mathbf{k},t) = C(\mathbf{k},-t), \tag{11}$$

$$C(\mathbf{k},t=0) = 0, \tag{12}$$

$$\dot{C}(\mathbf{k},t=0) = 0, \tag{13}$$

where dot denotes the time derivative. Expressions (12) and (13) reflect conservations of the normalization and the centre of gravity of the spectrum of $G_{\mathbf{k}}(t)$, respectively. Following the conventional nomenclature of the relaxation processes we may write

$$C(\mathbf{k},t) = C^{pol}(\mathbf{k},t) + C^{sat}(\mathbf{k},t) \tag{14}$$

with

$$C^{pol}(\mathbf{k},t) = -i\left[-\int_{-\infty}^{\infty}\frac{\rho(\mathbf{k},\omega)}{\omega}d\omega\right]t = -iv_{\mathbf{k}}t, \tag{15}$$

where $v_{\mathbf{k}}$ is the polarization induced energy shift, and

$$C^{sat}(\mathbf{k},t) = -\int_{-\infty}^{\infty}\rho(\mathbf{k},\omega)\frac{1-e^{-i\omega t}}{\omega^2}d\omega \tag{16}$$

is the satellite generator.

Taking the second time derivative of (8) we find

$$\ddot{C}(\mathbf{k},t) = -\int_{-\infty}^{\infty}\rho(\mathbf{k},\omega)e^{-i\omega t}d\omega \tag{17}$$

and by Fourier inversion

$$\rho(\mathbf{k},\omega) = -\frac{1}{2\pi}\int_{-\infty}^{\infty}\ddot{C}(\mathbf{k},t)e^{i\omega t}dt. \tag{18}$$

Hence, the cumulant spectrum $\rho(\mathbf{k},\omega)$ which carries information on the dynamics of coupled particle-field excitations in the interacting system described by the Hamiltonian (4) can be determined once the functional form of $C(\mathbf{k},t)$ in (5) is known. The reverse also holds true because expressions (8) and (18) are invertible (see Appendix A) and the exponential representation of the single particle propagator (5) is exact.

3. Reconstruction of cumulant representation from quasiparticle spectrum

3.1. Relation between the cumulant and standard spectral representations

Finding the form of $C(\mathbf{k},t)$, or alternatively of $\rho(\mathbf{k},\omega)$, is equivalent to solution of the many-body problem posed by the full Hamiltonian H. Therefore, apart from few exactly soluble models referred to above and explicitly illustrated below, approximate schemes for calculation of $C(\mathbf{k},t)$ or $\rho(\mathbf{k},\omega)$ should be employed to determine $G_{\mathbf{k}}(t)$. To establish the relation between the spectrum of the standard representation (7), as obtained e.g. from the Dyson equation for the propagator, and the excitation spectrum $\rho(\mathbf{k},\omega)$ of cumulant representation (8) we proceed as follows. We equate the last line of expression (5) with (7) which yields for $t \geqslant 0$

$$C(\mathbf{k},t) = \ln \int_{-\infty}^{\infty} \mathcal{N}(\mathbf{k},\omega') e^{-i(\omega'-\epsilon_{\mathbf{k}})t} d\omega'. \tag{19}$$

Defining the dynamical spectral moments

$$\mu_m(\mathbf{k},t) = \int_{-\infty}^{\infty} (\omega')^m \mathcal{N}(\mathbf{k},\omega') e^{-i\omega' t} d\omega' = i^m \frac{\partial^m}{\partial t^m} \mu_0(\mathbf{k},t) \tag{20}$$

and taking the time derivatives of (19) and manipulating with the resulting expressions we find:

$$-\ddot{C}(\mathbf{k},t) = \frac{\mu_2(\mathbf{k},t)}{\mu_0(\mathbf{k},t)} - \left[\frac{\mu_1(\mathbf{k},t)}{\mu_0(\mathbf{k},t)}\right]^2. \tag{21}$$

Hence, the knowledge of dynamical moments (20) of the quasiparticle spectrum $\mathcal{N}(\mathbf{k},\omega')$ enables the calculation of $\ddot{C}(\mathbf{k},t)$ and thereby of the cumulant spectrum $\rho(\mathbf{k},\omega)$ given by expression (18). The quotients in (21) should be treated with care because the real and imaginary parts of $\mu_0(\mathbf{k},t)$ may have common zeros in the case of total or complete collapse of the quasiparticle wavefunction for long times (cf. Eq. (35) and Fig. 10 below). Note also that the passage or mapping $\mathcal{N}(\mathbf{k},\omega') \to \rho(\mathbf{k},\omega)$ via Eqs. (21) and (18) allows to trace the development and representation of strong final state effects in $C(\mathbf{k},t)$ like the formation of bound states below the continuum [23,60], whereas it is not evident how this may be accomplished in reverse by starting from low order cumulant expansion [17].

The short time limit of (21) gives the square of inverse Zeno time τ_Z or Zeno convexity [61] which characterizes initial ballistic propagation of a quasiparticle upon its injection into the band [15,20,21], viz. the behaviour

$$C(\mathbf{k}, t \to 0) = -\frac{1}{2}\frac{t^2}{\tau_Z^2} + \mathcal{O}(t^3), \tag{22}$$

where $\tau_Z^{-2} = \int_{-\infty}^{\infty} \rho(\mathbf{k},\omega) d\omega$. This limit signifies that the early quasiparticle motion is not constrained to the energy shell because τ_Z depends only on the global properties of the band through its moments, but not on the initial state energy (cf. Ref. [70] and Section II of Ref. [20]). The energy conserving processes are established after the ballistic motion and early transients have died out and the steady state scattering regime reached [19]. Eventually, this intermediate steady state is succeeded by the quasiparticle collapse and transition into the asymptotic regime [58]. We shall demonstrate that the present approach enables the treatment of all such elementary stages of nonadiabatic quasiparticle dynamics and related spectral properties on an equivalent footing.

3.2. Derivations of cumulant representations for exactly solvable quasiparticle spectra

Major implications of expressions (8)–(22) can be best illustrated on some historically most exploited examples of solutions for the spectrum of a quasiparticle coupled to bosons. Here we consider several characteristic cases relevant to our further discussions of the general properties of quasiparticle propagators in the time domain.

3.2.1. Independent boson model spectrum

The first example is independent boson (IB) model [22,41,62] describing a single level of energy ϵ_0 coupled through the interaction strength $(v\omega_0)^{1/2}$ to a boson field of excitation energy ω_0. Hence

$$H_0^p = \epsilon_0 c^\dagger c, \tag{23}$$

$$H_0^b = \omega_0 a^\dagger a, \tag{24}$$

$$V = (v\omega_0)^{1/2} c^\dagger c(a + a^\dagger). \tag{25}$$

Then, $G^0(t) = -ie^{-i\epsilon_0 t}$ and the exact IB model spectrum is obtained in the form of Poisson distribution [22]

$$\mathcal{N}^{IB}(\omega') = e^{-\frac{v}{\omega_0}} \sum_{l=0}^{\infty} \frac{(v/\omega_0)^l}{l!} \delta(\omega' - \epsilon_0 + v - l\omega_0). \tag{26}$$

Using Eqs. (19)–(21) we find

$$\mu_0^{IB}(t) = e^{-i\epsilon_0 t} \exp[-(v/\omega_0)(1 - i\omega_0 t - e^{-i\omega_0 t})], \tag{27}$$

$$\rho^{IB}(\omega) = v\omega_0 \delta(\omega - \omega_0). \tag{28}$$

Here $v = \int d\omega \rho(\omega)/\omega > 0$ has the meaning of the quasiparticle energy relaxation shift. The prefactor e^{-v/ω_0} which weights the elastic ($l = 0$) and satellite lines ($l \geqslant 1$) of $\mathcal{N}^{IB}(\omega')$ has the appearance of the Debye–Waller factor (DWF).

3.2.2. Restricted Tamm–Dancoff spectrum

The IB model from Subsection 3.2.1 can be also solved approximately in the Tamm–Dancoff approximation (TDA). This amounts to calculating the quasiparticle propagator using the Dyson expansion in terms of the self-energy calculated to lowest (linear) order in v. This restricts the number of excited bosons in the intermediate quasiparticle states to zero or one. The result is a two-pole spectrum

$$\mathcal{N}^{TDA}(\omega') = Z_1 \delta(\omega - \epsilon_1) + Z_2 \delta(\omega - \epsilon_2) \tag{29}$$

with the renormalized quasiparticle peak energies given by $\epsilon_{1,2} = \epsilon_0 + \frac{\omega_0}{2} \mp \sqrt{\frac{\omega_0^2}{4} + v\omega_0}$. The ϵ_0-independent peak intensities $Z_{1,2} = \frac{1}{2}(1 \pm \sqrt{\omega_0/(\omega_0 + 4v)})$ satisfy the unitarity condition $Z_1 + Z_2 = 1$, and Z_1 is the analogue of the exact DWF. From this we obtain:

$$\mu_0^{TDA}(t) = e^{-i\epsilon_0 t}(Z_1 \exp[-i(\epsilon_1 - \epsilon_0)t] + Z_2 \exp[-i(\epsilon_2 - \epsilon_0)t]), \tag{30}$$

and the TDA cumulant spectrum is given by the infinite series

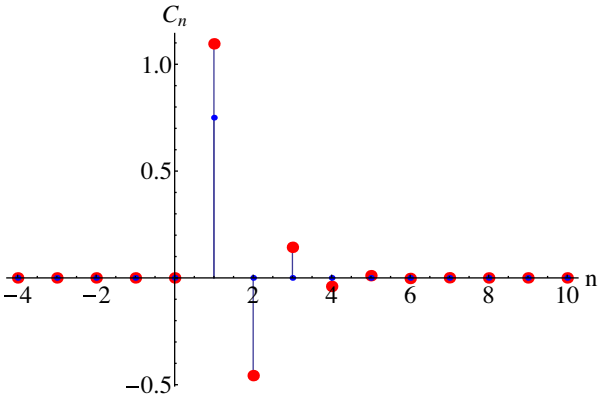

Fig. 1. Values of the coefficients C_n^{TDA} of the Tamm–Dancoff cumulant spectrum (31) for the IB model parameters $\epsilon_0 = 1$, $v = 1/2$ and $\omega_0 = 3/2$. Note that $C_n^{TDA} = 0$ for $n \leqslant 0$. The value of $C_{n=1}^{IB}$ of the generic IB cumulant spectrum (28) is indicated by lower small dot at $n = 1$, whereas all other $C_{n\neq 1}^{IB} = 0$.

$$\rho^{TDA}(\omega) = \sum_{n=-\infty}^{\infty} C_n^{TDA}\delta(\omega - n\Omega_0) \tag{31}$$

with the period $\Omega_0 = (\epsilon_2 - \epsilon_1) = \omega_0\sqrt{1 + 4v/\omega_0}$. The coefficients C_n^{TDA} are obtainable in analytical albeit complicated form involving combinations of hypergeometric functions. The variation of C_n^{TDA} with n for a particular choice of IB model parameters is shown in Fig. 1. In contrast, the series for exact $\rho^{IB}(\omega)$ with the period ω_0 contains only one term $C_{n=1}^{IB} = v\omega_0 > 0$ [cf. Eq. (28)].

There are several important implications of the TDA solution (29)–(31) of the exactly soluble IB model of Subsection 3.2.1. The TDA generates a downward (red) polarization shift of the threshold spectral level at $\omega = \epsilon_1$, in accord with the properties of IB-spectrum (26). However, it generates an upward (blue) relaxation shift of the satellite at $\omega = \epsilon_2$ which is in contradiction with the exact red shift v of all the levels in the IB model (26). This is a consequence of restricting the excitation dynamics to a single boson propagation in the intermediate states which must compensate for the excitation energy and spectral weight of higher order excitations excluded from the TDA description of system dynamics. In turn, this results in the cumulant spectrum (31) in the form of an infinite series with alternating sign of the constituting terms, in contrast to the strictly positive expression (28) obtained from the exact solution for the IB model spectrum. Since the GW approximation is equivalent to Tamm–Dancoff approximation for the retarded screened Coulomb interaction, it may be inferred that the spectral satellite structure calculated within the GWA approach may exhibit similar deficiencies as found in the present simple example. This was clearly corroborated in Ref. [30] which illustrates that hot electron dynamics may not be adequately described within the GWA.

3.2.3. Infra-red power law spectrum

The third example is the threshold or infra-red (IR) power law spectrum [53] typical of the interactions of localized particles with bosons exhibiting linear density of excitations for $\omega \to 0$. The appropriate expression for the spectrum exhibiting IR power law behaviour is [62]

$$\mathcal{N}^{IR}(\omega') = \frac{e^{-(\omega' - \epsilon_0 + v)/\Delta}\theta(\omega' - \epsilon_0 + v)}{\Delta^{\beta}\Gamma(\beta)(\omega' - \epsilon_0 + v)^{1-\beta}}, \tag{32}$$

where $\beta > 0$, $v > 0$, $\Delta = v/\beta$ and $\Gamma(\beta)$ are the critical IR exponent, energy relaxation shift, excitation energy bandwidth, and the Gamma function, respectively. Here the DWF is zero and hence $\mathcal{N}^{IR}(\omega')$ comprises the inelastic wing only. Using (19)–(21) we find

$$\mu_0^{IR}(t) = e^{-i(\epsilon_0 - v)t}(1 + i\Delta t)^{-\beta}, \tag{33}$$

$$\rho^{IR}(\omega) = \beta\omega e^{-\omega/\Delta}\theta(\omega). \tag{34}$$

Note that in the IB and IR models there exists a well defined red-shifted spectral threshold (band bottom) at $\omega' = \epsilon_0 - v$. The same applies to convolutions of the IB and IR spectra. Also, in contrast to the TDA cumulant spectrum (31) both $\rho(\omega)$ given by (28) and (34), as well as their convolution, are real positive functions.

3.2.4. General form of the cumulant representation

Information on the electron evolution subsequent to injection into an empty band is contained in two complementary quantities, the quasiparticle survival probability

$$L(\mathbf{k}, t) = |G_{\mathbf{k}}(t)|^2 = |\mu_0(\mathbf{k}, t)|^2 \tag{35}$$

and the quasiparticle phase

$$\varphi(\mathbf{k}, t) = -\Im \ln(iG_{\mathbf{k}}(t)) = \epsilon_{\mathbf{k}}^0 t + \delta\varphi(\mathbf{k}, t) = \epsilon_{\mathbf{k}}^0 t - \Im C(\mathbf{k}, t). \tag{36}$$

In this notation the derivative $\partial\delta\varphi(\mathbf{k}, t)/\partial t = \delta\epsilon_{\mathbf{k}}^0(t)$ describes the relaxation of quasiparticle energy in the course of time.

To extract relevant information on the quasiparticle evolution using definitions (35) and (36) we first observe that in the paradigmatic examples of Subsections 3.2.1, 3.2.2 and 3.2.3 the simple analytical invertibility $\mathcal{N}(\omega') \leftrightarrow \rho(\omega)$ is facilitated by the simple functional forms of $\rho(\omega)$ for which

$\rho(\omega \leqslant 0) = 0$. In such cases the survival probability (35) describes initial ballistic propagation $L(\mathbf{k},t) \sim \exp(-t^2/\tau_Z^2)$ arising from (22), which then goes over either into unattenuated oscillatory behaviour (IB and TDA model) or a power law decay (IR model), but the respective forms of $\rho(\omega)$ do not give rise to an exponential quasiparticle decay $L(\mathbf{k},t) \propto \exp(-2\Gamma_{\mathbf{k}}t)$ during any interval of propagation. In order that such a decay governed by the on-the-energy-shell transition rate $\Gamma_{\mathbf{k}}$ takes place in the preasymptotic region it is necessary that $\rho(\mathbf{k},\omega = 0^{\pm}) > 0$. In that case

$$C(\mathbf{k}, t \gg \tau_Z) \simeq -w_{\mathbf{k}} - iv_{\mathbf{k}}t - \Gamma_{\mathbf{k}}t + f(\mathbf{k},t), \tag{37}$$

where $w_{\mathbf{k}}$ is a complex constant yielding the Debye–Waller exponent for the quasielastic (QE) quasiparticle line in the spectrum

$$w_{\mathbf{k}} = \int_{-\infty}^{\infty} \frac{\partial\rho(\mathbf{k},\omega)}{\partial\omega}\frac{d\omega}{\omega}, \tag{38}$$

the next pure imaginary term on the RHS of (37) comprises the real energy shift $v_{\mathbf{k}}$ defined in (15), and

$$\Gamma_{\mathbf{k}} \simeq \pi\rho(\mathbf{k},0) \tag{39}$$

yields the inverse lifetime $\tau_{\mathbf{k}}^{-1} = (2\Gamma_{\mathbf{k}})$ of the quasiparticle initial state $|\mathbf{k}\rangle$. The remaining function $f(\mathbf{k},t)$ may comprise the terms exhibiting logarithmic, inverse power and oscillatory temporal behaviour, the latter arising from the prominent maxima in $\rho(\mathbf{k},\omega)$. Each of the terms in (37) is characterized by its own onset time and hence the treatment of all quasiparticle evolution stages and ensuing spectral properties requires a careful assessment of the mapping $\rho(\mathbf{k},\omega) \to \mathcal{N}(\mathbf{k},\omega')$ and vice versa.

3.3. Representation of distinct stages of quasiparticle evolution in multiexcitation processes

The quasiparticle spectrum $\mathcal{N}(\mathbf{k},\omega')$ and the cumulant excitation spectrum $\rho(\mathbf{k},\omega)$ contain equivalent information on the quasiparticle dynamics and decoherence. However, from the practical point of view the two complementary representations of the propagator, viz. expressions (5) and (7), do not prove equally convenient in extracting specific aspects of excitation dynamics in distinct energy or temporal intervals even in the case of the same system. Thus, as has already been pointed out above, the calculations of $\mathcal{N}(\mathbf{k},\omega')$ for the coupled particle–boson system the standard approximate approaches based on perturbative and equations of motion methods may give unsatisfactory results as regards the multiple excitation structure in the spectral region above the quasielastic peak. By contrast, second order cumulant expansion provides a reliable description of the dynamics of a particle coupled to bosons in the preasymptotic evolution intervals [19,54], and reduces to exact solutions in the limit of infinitely narrow bands [41,45,62] [cf. Eqs. (26) and (32)], and in the opposite limit of infinitely wide bands with linear dispersion of quasiparticle energy [22]. The reliable coverage of these two extreme energy intervals implies reliable description of multiexcitation and elementary decay processes that determine the early and intermediate quasiparticle evolution intervals. However, the regime of asymptotic or long time quasiparticle evolution characterized by the wavefunction collapse and subsequent nonexponential decay [58] may not be easily retrieved from the representation (5), again except for very few cases of exactly solvable models. Derivation of the asymptotic quasiparticle evolution that depends on the spectral characteristics near the band bottom may favour calculations of the propagator directly from expression (7) provided the spectral shape in that region can be sufficiently accurately assessed either by perturbative or nonperturbative methods.

Combining and extending the results of Sections 2 and 3.1 we can propose a procedure for construction of the propagators describing quasiparticle dynamics in the band that encompasses all distinct temporal stages of quasiparticle evolution. To this end we exploit in the first step the advantages of cumulant approach and calculate $\exp[C(\mathbf{k},t)]$ using low order cumulant expansion in powers of the interaction V. As illustrated in several works [17,19,26,37,54], for the majority of physical systems of interest this amounts to representing (8) by the second order cumulant $C_2(\mathbf{k},t)$ calculated from $\rho_2(\mathbf{k},\omega)$ that is quadratic in V. The thus obtained propagators $G(\mathbf{k},t)$ combine the effects of initial ballistic propagation, multiple excitation of the heatbath and concomitant preasymptotic exponential decay of the quasiparticle initial state that is governed by the Fermi golden rule (FGR) lifetime $\sim 1/2\pi\rho_2(\mathbf{k},0)$. This procedure yields the quasiparticle spectra $\mathcal{N}(\mathbf{k},\omega')$ with correct positions, weights

and lineshapes of the quasielastic (QE) peak and satellite structure [22], but misses out the proper description of spectral features near the band bottom which controls the asymptotic quasiparticle decay [58]. Instead, due to the absence of phase space correlations in second order cumulant approximation, it introduces a spectral tail [63] that smoothly extends across the lower band edge fixed by the absolute minimum of the renormalized energy dispersion curve

$$\tilde{\epsilon}_{\mathbf{k}} = \epsilon_{\mathbf{k}} + v_{\mathbf{k}}. \tag{40}$$

The unphysical spectral tail below the band bottom of (40) should be removed by introducing some suitable and physically motivated cutoff below the QE peak [64] (we assume that the latter does not coincide with the band bottom). In the next step we add to the thus truncated cumulant spectrum the band bottom component of the spectrum $\mathcal{N}(\mathbf{k},\omega')$ calculated perturbatively and cut off at the same energy below the QE peak. The reliability of this procedure depends on the accuracy of description of the spectral shape near the band bottom by perturbation theory. By contrast, the tail in the ultraviolet region is physical and not critical from the convergence point of view because the high energy component of cumulant-derived spectrum usually exhibits strong attenuation and finite moments of the satellite structure [65].

Outside the limits of very narrow or wide quasiparticle bands a convenient procedure to obtain the desired band bottom correction with required accuracy is the use of simple or generalized GWA [25–27,44]. This approximation tends to yield the correct energy shift and spectral intensity at the threshold, like the simple TDA discussed in Section 3.2.2. The thus reconstructed threshold behaviour in combination with the poles of the spectrum gives rise to quasiparticle collapse and nonexponential asymptotic decay [58]. Since the cumulant representation of the propagator (5) using (8) predicts a universal form for the threshold and satellite shifts (15) in the spectrum of a $|\mathbf{k}\rangle$-state the choice of specific GWA should optimally reflect this feature. We write the GWA quasiparticle spectrum consistent with this requirement in the form

$$\mathcal{N}^{GWA}(\mathbf{k},\omega') = \frac{\Gamma_2(\mathbf{k},\omega')/\pi}{(\omega' - \epsilon_{\mathbf{k}} - \Lambda_2(\mathbf{k},\omega'))^2 + \Gamma_2(\mathbf{k},\omega')^2}, \tag{41}$$

where $\Sigma_2(\mathbf{k},\omega') = \Lambda_2(\mathbf{k},\omega') - i\Gamma_2(\mathbf{k},\omega')$ is the quasiparticle self-energy with the real and imaginary parts quadratic in the interaction V. Here we are interested in the application of (41) to description of the quasiparticle spectrum near the excitation threshold (small ω near the band bottom) which reproduces the long time behaviour of (5). In this limit the relevant quasiparticle energies have been relaxed (renormalized) by polarization of the boson field to the form (40). In accord with the applicability of the second order cumulant expansion we shall furthermore assume a weak variation of expression (15) with $\mathbf{k}$ in the region of interest, i.e. $v_{\mathbf{k}} \simeq v_{\mathbf{k}-q}$ and hence $\tilde{\epsilon}_{\mathbf{k}-\mathbf{q}} - \tilde{\epsilon}_{\mathbf{k}} \simeq \epsilon_{\mathbf{k}-\mathbf{q}} - \epsilon_{\mathbf{k}}$. Then, in analogy with the core level problem of Ref. [44] in which these relations are exactly fulfilled, as well as with Hedin's Ansatz for GW self-energy [26], we write

$$\Sigma_2(\mathbf{k},\omega') = \int_{-\infty}^{\infty} dv \frac{\tilde{\rho}_2(\mathbf{k},v)}{\omega' - \tilde{\epsilon}_{\mathbf{k}} - v + i\delta}. \tag{42}$$

Here $\tilde{\rho}_2(\mathbf{k},v)$ is expressed in terms of the relaxed energies $\tilde{\epsilon}$'s in order to eliminate the pole at $\tilde{\epsilon}_{\mathbf{k}}$ in the integrand on the RHS of (42) and to introduce a continuum of new ones at $\tilde{\epsilon}_{\mathbf{k}-\mathbf{q}}$. The real and imaginary part of the self-energy (42) are related through the Hilbert transform

$$\Lambda_2(\mathbf{k},\omega') = \frac{1}{\pi}\int_{-\infty}^{\infty} \frac{\Gamma_2(\mathbf{k},v)}{\omega' - v} dv. \tag{43}$$

In this representation the weight of the QE peak in the spectrum appears in the form

$$Z_{\mathbf{k}} = \left(1 + \frac{\partial \Lambda_2(\mathbf{k},\omega')}{\partial \omega'}|_{\omega'=E_{\mathbf{k}}}\right)^{-1}, \tag{44}$$

where the relaxed QE peak energy $E_{\mathbf{k}} = \tilde{\epsilon}_{\mathbf{k}}$ is the first root [66] of $\omega' - \epsilon_{\mathbf{k}} - \Lambda_2(\mathbf{k},\omega') = 0$ above the band bottom given by the minimum value(s) of (40).

Now we are in a position to establish connections between the GWA quantities in (41) and those defining the cumulant $C_2(\mathbf{k},t)$ calculated to the same order in V [67]. Using (15) and (43) we find the relation between the relaxation energy of QE spectral peak in the cumulant and the above constructed GWA representation

$$\Lambda_2(\mathbf{k},\tilde{\epsilon}_{\mathbf{k}}) = v_{\mathbf{k}}. \tag{45}$$

In a similar fashion, a comparison with (38) yields

$$Z_{\mathbf{k}} = 1 - \Re w_{\mathbf{k}}. \tag{46}$$

Finally, from (42) we directly find

$$\Gamma_2(\mathbf{k},\omega') = \pi\rho_2(\mathbf{k},\omega' - \tilde{\epsilon}_{\mathbf{k}}). \tag{47}$$

Hence, the full width at half maximum (FWHM) of the QE peak, or equivalently the inverse quasiparticle lifetime $\tau_{\mathbf{k}}^{-1}$, is given by $2\Gamma_2(\mathbf{k},\tilde{\epsilon}_{\mathbf{k}})$.

It is seen from expressions (45)–(47) that the quantities appearing in the GWA representation (41) are referred to the relaxed energies $\tilde{\epsilon}$. Hence, this representation should prove useful in modelling the threshold spectral properties of quasiparticles in image potential states on metal surfaces because the calculated image potential band structures [68] already include the effects of electronic polarization that gives rise to the relaxation shift $v_{\mathbf{k}}$.

For the present purpose of introducing the missing threshold spectral properties into the second order cumulant-derived spectrum one may introduce smooth cut-offs of the cumulant and GWA components in order to avoid unphysical transients arising from the cusped or discontinuous seams. The precise value of cut-off energy is not important for the functional form of asymptotic decay because expression (21) is insensitive to normalization of the spectrum $\mathcal{N}(\mathbf{k},\omega')$. However, the position of cut-off can affect the collapse onset time. In some situations this procedure may produce an accurate total spectrum provided the cut-offs have been implemented such to provide a unitary and smooth juxtaposition of two spectral components. Specifically, this would occur if the weight of QE peak in the GWA spectrum is very close to the DWF of cumulant expansion, as is the case for $\Re w_{\mathbf{k}} \ll 1$. If the weights are significantly different, i.e. if the straightforward spectral juxtaposition procedure violates unitarity one should in the third step rescale the GWA weight of the QE peak to the DWF using (46) and substitute the sum of two spectral components into (20) to yield spectral moments which via Eqs. (21) and (8) determine the full quasiparticle propagator (5) and the corresponding spectrum. Likewise in the benchmark examples of Section 3.2 we thereby achieve that the calculated quasiparticle propagator and its spectrum comprise dynamical effects from the entire evolution interval and exhibit unitary spectral properties. An alternative approach to the calculation of quasiparticle spectrum followed in Ref. [37] and its relation to the present one is commented in Appendix B.

4. Model examples of quasiparticle dynamics in surface bands

In this section we illustrate and test the applicability of developed formalism using the models of general relevance to hot electron dynamics in Q2D surface bands. Typical examples of Q2D bands are the image potential bands (IS-bands) which arise on low index surfaces of a number of fcc and bcc metals [69]. Since the IS-bands originate from a combined effect of the surface crystal structure and dynamic electronic polarization of the metal, their formation proceeds on the sub- or few femtosecond time scale subsequent to the electron promotion in front of the surface (for illustration of time scale of IS-band formation on Cu surface see Fig. 5 in Ref. [71] and Figs. 5 and 6 in Ref. [72]). In this case the propagator formalism described in Sections 2 and 3 and based on the assumption of creation of an electron in a band state lends itself as a convenient approach to study the evolution and decoherence of quasiparticles in the real time domain. The forthcoming discussion will be restricted only to the general and qualitative aspects of multiexcitation processes switched on with the promotion of quasiparticles into IS-band states. The applications to electron dynamics at surfaces of real metals will be pursued in the future work by combining the band structure calculations with the linear response formalism elaborated in Ref. [19].

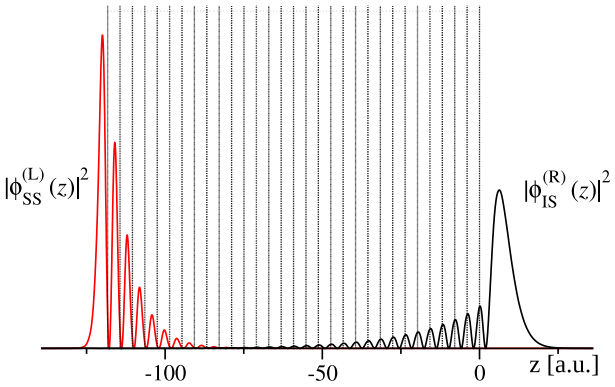

Fig. 2. Plot of absolute squares of the wavefunctions yielding electron densities residing in the Shockley surface state, $|\phi_{SS}^{(L)}(z)|^2$, on the left (1 1 1) surface, and in the first image potential state, $|\phi_{IS}^{(R)}(z)|^2$, on the right (1 1 1) surface of a 31 atomic layer thick Cu slab (shaded region) with interlayer spacing $d_0 = 3.943$ a.u.

We first outline the general features of quasiparticle dynamics in Q2D bands on metal surfaces. The unperturbed electron eigenstates are characterized by a two-dimensional wavevector **K** parallel to the surface and the band index n, viz. $\mathbf{k} = (\mathbf{K}, n)$ and $\langle \mathbf{r}|\mathbf{k}\rangle = \exp(i\mathbf{KR})\phi_n(z)$. In Fig. 2 we illustrate the occupied Shockley surface state (SS) wavefunction $\phi_{n=SS}(z)$ and the unoccupied first image potential state wavefunction $\phi_{n=IS}(z)$ calculated for a 31 atomic layer thick crystal slab which we use to model the electronic properties of Cu (1 1 1) surface [19]. The dominant interaction acting on an electron injected into an empty band state $|\mathbf{K}, n\rangle$ arises from the coupling to electronic charge density fluctuations in the slab which are described by the 2D wavevector **Q** and excitation energy v. Restricting the description of the interaction to linear response, which is equivalent to bosonization of the electron interaction with the heatbath, we obtain the cumulant spectrum $\rho_2(\mathbf{K}, n, \omega)$ from (9) in the form [17]

$$\rho_2(\mathbf{K}, n, \omega) = \sum_{\mathbf{Q},n'} |V_{\mathbf{Q}}|^2 \int_0^\infty \mathcal{S}_{n,n';n',n}(\mathbf{Q}, v)\delta(\omega - \epsilon_{\mathbf{K}+\mathbf{Q},n'} - v + \epsilon_{\mathbf{K},n})dv. \tag{48}$$

This is a positive definite quantity in which $V_{\mathbf{Q}} = 2\pi e^2/Q$ is a 2D Fourier transform (FT) of the Coulomb potential and $\mathcal{S}_{n,n';n',n}(\mathbf{Q}, v)$ is the spectrum of bosonic charge density fluctuations obtained from the projection of the imaginary part of linear response function $\chi(\mathbf{Q}, z, z', v)$ onto the one-electron wavefunctions $\phi_n(z)$ and $\phi_{n'}(z)$ in the Q2D bands. Derivation and discussions of the properties of $\chi(\mathbf{Q}, z, z', v)$ and $\mathcal{S}_{n,n';n',n}(\mathbf{Q}, v)$ were presented in Section II of Ref. [19]. In brief, on metal surfaces the excitations

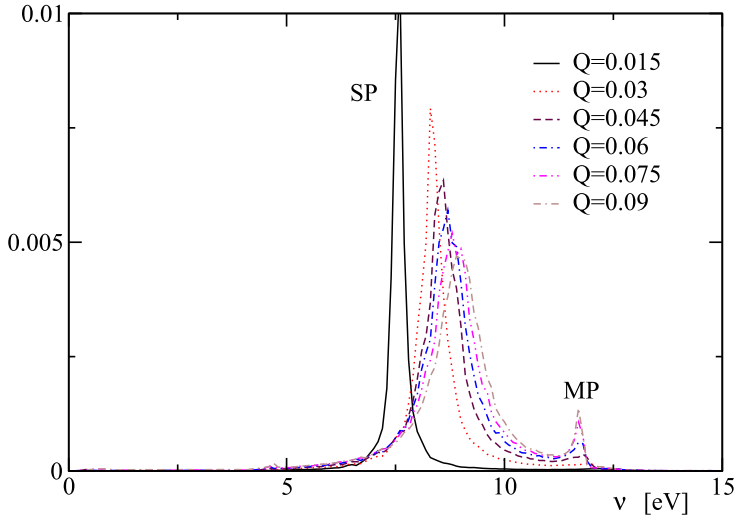

Fig. 3. First image state intra-band component of the excitation spectrum $\mathcal{S}_{IS,IS;IS,IS}(\mathbf{Q}, v)$ for several values of Q. SP and MP denote the peaks associated with monopole surface plasmon and higher order multipole plasmon mode, respectively.

constituting $\mathcal{S}_{n,n';n',n}(\mathbf{Q},v)$ are the monopole plasmon excitations with energies in the range $3-13$ eV, multipole plasmons with few eV higher energies but smaller weight (i.e. oscillator strength), whereas the strongly $\mathbf{Q}$-dependent electron–hole continuum ranges from zero up to the plasmon energies and beyond, with a maximum around $v \simeq Qv_F$ (v_F is the Fermi velocity). Fig. 3 illustrates the behaviour of IS-state intraband component of $\mathcal{S}_{\mathrm{IS,IS;IS,IS}}(\mathbf{Q},v)$ calculated for Cu (1 1 1) surface using the slab wavefunctions $\exp(i\mathbf{KR})\phi_n(z)$. Note that $\rho_2(\mathbf{K},n,\omega)$ obtained from (48) ranges over the complete spectrum of excitation processes in the system that are quadratic in the interaction (3), viz. it encompasses both the virtual or off-the-energy shell ($\omega \neq 0$) and the on-the-energy shell ($\omega = 0$) components. Therefore $\rho_2(\mathbf{K},n,\omega)$ may be identified with the interaction weighted density of excitations in the system.

4.1. Quasiparticle excited to the band bottom $\mathbf{K} = 0$

We first consider simpler situation in which the particle is promoted into a state $\epsilon_{\mathbf{K}=0} = 0$ at the bottom of the nth surface band [73]. In order to discern and assess the specificities of the dynamics associated with this state we shall in the following exclude interband transitions $n' \neq n$ from the sum on the RHS of (48), which is also consistent with the starting assumption of a single band made in Section 2. Interband transitions redistribute the quasiparticle spectral features over the lower unoccupied bands closer to the Fermi level and their effects will be briefly outlined at the end of this section. The initial electron kinetic energy at the band bottom is zero which defines the excitation threshold of $\rho(\mathbf{K}=0,n,\omega)$ at $\omega = 0$. It is known from the earlier studies [43] that in this case $\rho_2(\mathbf{K}=0,n,\omega\to 0) \propto \omega^2$ and as a consequence the quasiparticle spectrum $\mathcal{N}(\mathbf{K}=0,\omega')$ exhibits an elastic threshold peak $\propto \delta(\omega' + v_0)$ at the renormalized (red-shifted) band bottom energy $\omega' = -v_0$, and an inelastic sideband which starts from a finite value for $\omega' = -v_0$. The elastic peak exhibits zero width $\Gamma(\mathbf{K}=0) = 0$ because of the absence of open channels through which at zero temperature the quasiparticle may decay into the states of other energies. In contrast to this, the wide inelastic sideband arises as a result of an infinite series of ascending numbers of convolutions of the single boson excitation spectra, in full analogy with expressions (26) and (32). Apart from an overall scaling or Debye–Waller factor the threshold behaviour of the sideband is determined solely by the low-energy excitations. Hence, in the present example we shall neglect the contribution of plasmons to (48) and focus only on the effects which the continuous or electron–hole (e–h) pair component of the surface electronic response produces in the quasiparticle spectrum [74]. This enables us to demonstrate the invertibility of mapping $\rho(\mathbf{K},\omega) \leftrightarrow \mathcal{N}(\mathbf{K},\omega')$ using a nontrivial and highly illustrative, but exactly solvable analytical model.

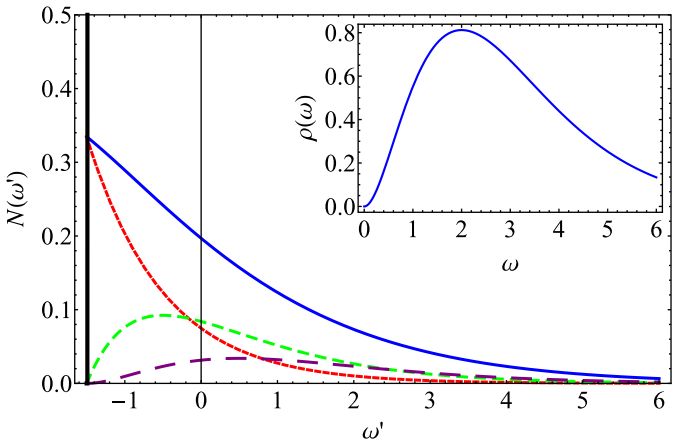

Fig. 4. Plots of the quasiparticle spectrum $\mathcal{N}^{e-h}(\mathbf{K}=0,\omega')$ defined in Eq. (49), and its components (sub-sidebands), for $\bar{\varepsilon} = 3/2$, $\Delta = 1$ and $\Omega = 1$. Energy unit is Ω and zero corresponds to the unperturbed electron energy $\epsilon_{\mathbf{K}=0} = 0$. Vertical thick line: elastic threshold peak, full line: complete sideband. Short dashed line, intermediate dashed line and long dashed line denote $n = 1, 2, 3$ sub-sidebands, respectively. Inset: Corresponding cumulant spectrum (51) obtained by inversion of (49) as described in Section 3.1.

To quantify the above discussion and, in particular, to examine the role of band bottom effects on the cumulant spectrum (18), we introduce a convenient representation of the quasiparticle spectrum comprising bosonized e–h pair multiexcitation processes in the form

$$\mathcal{N}^{e-h}(\mathbf{K}=0,\omega') = e^{-\bar{\varepsilon}\Delta/\Omega^2}\left[\delta(\bar{\omega}') + \frac{\exp(-\bar{\omega}'/\Delta)\sqrt{\bar{\varepsilon}\bar{\omega}'}I_1(2\sqrt{\bar{\varepsilon}\bar{\omega}'}/\Omega)}{\bar{\omega}'\Omega}\right], \tag{49}$$

where $\bar{\omega}' = \omega' + v_0$, $v_0 = \bar{\varepsilon}(\Delta/\Omega)^2$, and $I_1(x)$ is the modified Bessel function of the first kind and the parameters $\bar{\varepsilon}$, Δ and Ω have the meaning of the averaged single boson excitation energy, band width and energy scale, respectively. The universal form of the spectrum (49) is chosen such that it represents the elastic threshold peak $\exp(-\bar{\varepsilon}\Delta/\Omega^2)\delta(\bar{\omega}')$ followed by a series of ascending convolutions of the boson excitation events which are obtained by expanding the Bessel function on the RHS of (49) into a power series. The overall prefactor $\exp(-\bar{\varepsilon}\Delta/\Omega^2) < 1$ plays the role of the Debye–Waller factor which ensures the correct normalization of the spectrum, and $\exp(-\bar{\omega}'/\Delta)$ is a smooth ultraviolet cutoff. The sideband spectral density and its few lowest components (sub-sidebands) are illustrated in Fig. 4 for the values of scaled parameters $\bar{\varepsilon}/\Omega$ and Δ/Ω typical of the intermediate coupling regime. In this case the Debye–Waller exponent $w_0 = \bar{\varepsilon}\Delta/\Omega^2$ is of the order of unity and hence the elastic threshold peak and the sideband bear approximately the same weight. The other regimes are described by simple rescaling of the quantities $\bar{\varepsilon}/\Omega$ and Δ/Ω. Thus, in the weak coupling regime $w_0 \ll 1$ the elastic peak represents the dominant spectral structure since the sideband bears negligible weight. In the opposite regime of strong coupling characterized by $w_0 \gg 1$ the elastic peak acquires negligible weight and the sideband turns into a normalized Gaussian centred at $\mu_1(\mathbf{K}=0,t=0)$. The main contribution to such Gaussian spectral density comes from the boson excitation processes with multiplicity of the order of w_0.

Inversion of the spectrum (49) defined through expressions (17)–(21) yields

$$\ddot{C}(\mathbf{K}=0,t) = -\frac{2\bar{\varepsilon}\Delta^3}{\Omega^2(1+i\Delta t)^3}, \tag{50}$$

and therefrom (see inset in Fig. 4)

$$\rho(\mathbf{K}=0,\omega) = \bar{\varepsilon}\left(\frac{\omega}{\Omega}\right)^2 e^{-\omega/\Delta}\theta(\omega). \tag{51}$$

This expression clearly reveals the physical significance of the parameters $\bar{\varepsilon}$, Ω and Δ for the cumulant excitation spectrum (9). Expressions (49)–(51) also support the earlier conjectures [43] on the general properties of $\rho(\mathbf{K}=0,\omega)$ and $\mathcal{N}(\mathbf{K}=0,\omega')$ at low excitation energies. The dynamical spectral moments

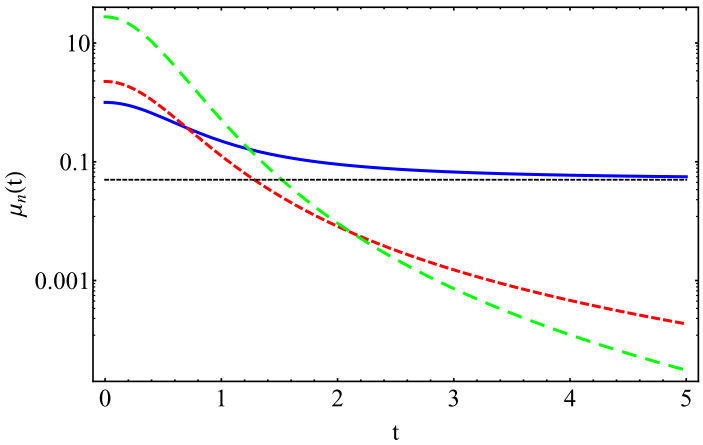

Fig. 5. Plots of the dynamical spectral moments $\mu_0(\mathbf{K}=0,t)$ (full line), $\mu_1(\mathbf{K}=0,t)/\Omega$ (short dashed line) and $\mu_2(\mathbf{K}=0,t)/\Omega^2$ (long dashed line) derived from spectrum in Fig. 4. The zeroth moment $\mu_0(\mathbf{K}=0,t)$ is equal to the quasiparticle survival probability defined in Eq. (35). Horizontal thin dashed line is the value of squared Debye–Waller factor. Note logarithmic scale on the vertical axis.

$\mu_n(\mathbf{K}=0,t)$ acquire analytical forms and the temporal variations of absolute squares of the first three ones needed in the calculation of $\rho(\mathbf{K}=0,\omega)$ are illustrated in Fig. 5. According to (35) the quasiparticle survival probability $L(\mathbf{K},t)$ is equal to the absolute square of $\mu_0(\mathbf{K}=0,t)$. Since in the present example $\Gamma(\mathbf{K}=0)=0$, the survival probability goes over from a ballistic directly to a power law decay and finally saturates at the value of the squared DWF. The reverse mapping also holds, substitution of (51) in (8) gives after some manipulation with the Fourier transforms of the results of integration the starting multiexcitation spectrum (49). It should be noted that the above invertible mappings $\rho \leftrightarrow \mathcal{N}$ reproduce and preserve correct threshold features of both quantities, which will prove important for the case $\mathbf{K}>0$ studied below. Analogous properties can be established also for other forms of quasiparticle spectra exhibiting similar functional behaviour.

4.2. Quasiparticle excited to a state with $\mathbf{K}>0$

Here we generalize the situation from the preceding subsection to the case in which the electron is promoted into a band state with $\mathbf{K}>0$. This requires taking into account the full spectrum of surface excitations embodied in $\mathcal{S}_{n,n';n',n}(\mathbf{Q},\nu)$. Likewise before we restrict the quasiparticle propagation to a single empty nth band, i.e. consider only the intraband contributions $n'=n$ to (48). Employing again the general arguments one finds [43] that for $\mathbf{K}>0$ the intraband component of the cumulant spectrum $\rho_2(\mathbf{K},n,\omega)$ vanishes below the excitation threshold now located at $\omega=-\epsilon_{\mathbf{K}}$, passes through a finite value at $\omega=0$ which determines the decay rate (39) characteristic of on-the-energy-shell excitation processes, and may reach a maximum near the energy (frequency) of each prominent peak of $\mathcal{S}_{n,n;n,n}(\mathbf{Q},\nu)$.

As the general features of the spectra of electronic charge density excitations at surfaces of a number of metals are relatively well known [75], we shall first construct a representative model expression for $\rho_2(\mathbf{K},n,\omega)$ which would optimally reflect the effects of excitation of e–h pairs and collective modes on the hot electron spectrum $\mathcal{N}(\mathbf{K},\omega')$. Since in the present case there is no single energy scale to appropriately describe all types of surface electronic excitations [i.e. there is no counterpart of Ω from Eq. (49)] we shall for illustrational purposes adopt a representation of the model $\rho_2(\mathbf{K},n,\omega)$ obtained by using (48) with $\mathcal{S}_{n,n;n,n}(\mathbf{Q},\nu)$ calculated for Cu (1 1 1) slab and illustrated in Fig. 3. Substituting this form of $\mathcal{S}_{n,n;n,n}(\mathbf{Q},\nu)$ into (48) we obtain $\rho_2(\mathbf{K},n,\omega)$ well suited for illustration of the effects of electronic heatbath modes on the electron spectrum $\mathcal{N}(\mathbf{K},\omega')$. However, it should be noted that the quantitative features of such restricted $\rho_2(\mathbf{K},n,\omega)$ have been selected to best illustrate gross aspects of electron coupling to the surface response and hence may not fully represent a real copper substrate with its peculiar electronic structure [76].

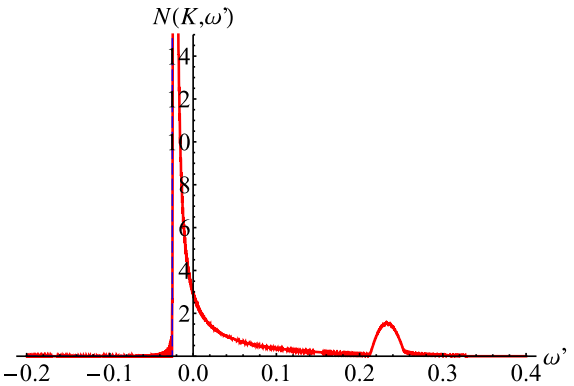

Fig. 6. Quasiparticle spectrum $\mathcal{N}(\mathbf{K},\omega')$ computed from cumulant representation (5) with the cumulant spectrum (48) for parameters typical of the first IS-band on Cu (1 1 1) and initial $K=0.06$ a.u. ($\epsilon_{\mathbf{K}}=47$ meV). Energies on the horizontal axis measured in a.u. (1 a.u. = 27.2 eV). Energy zero corresponds to the first static moment of the spectrum. The first satellite peak centred at 0.23 a.u. appears approximately at the surface plasmon energy above the quasielastic peak. For location of the spectral threshold, which on this scale is hardly discernable from the left slope of quasielastic peak, see Fig. 7. In the present weak coupling regime only the first plasmon satellite is visible.

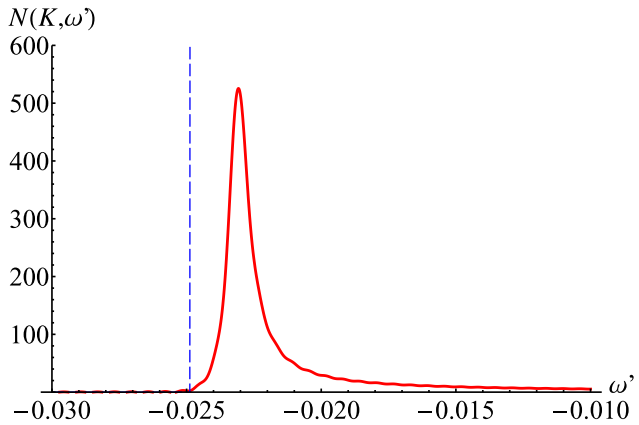

Fig. 7. Threshold behaviour of the quasiparticle spectrum from Fig. 6 shown on the expanded horizontal and reduced vertical scale. Full line is the spectral density computed from cumulant expansion. Thin dashed vertical line denotes the cut off energy that fixes the GWA spectral threshold. The unphysical spillover of the cumulant-derived spectral density below the threshold has negligible weight.

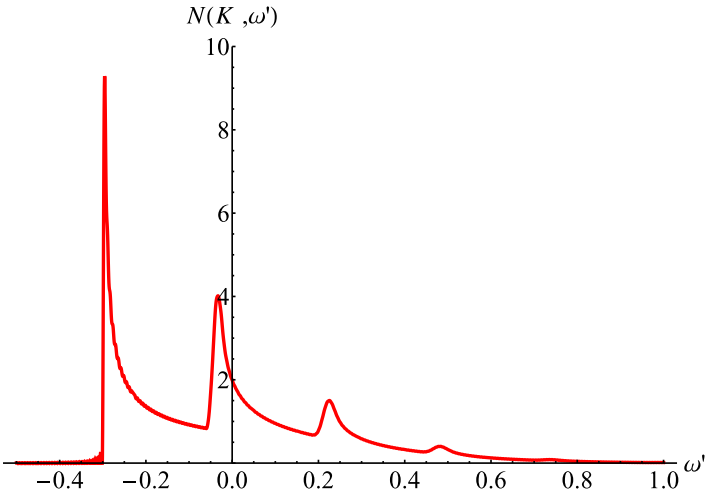

Fig. 8. Quasiparticle spectrum $\mathcal{N}(\mathbf{K},\omega')$ computed using the cumulant spectrum as in Fig. 6 but rescaled by a factor of 8. This leads to the intermediate coupling regime in which the satellite peaks appear approximately at multiples of the surface plasmon energy above the energy of quasielastic peak. Energy zero corresponds to the first static moment of the spectrum.

We now substitute the thus constructed model cumulant spectrum $\rho_2(\mathbf{K},n,\omega)$ into (8) to calculate the spectrum $\mathcal{N}(\mathbf{K},\omega')$ of an electron injected with momentum $\mathbf{K} > 0$ into a Q2D band with the characteristics of the first IS-band on Cu (1 1 1) surface. Following the procedure described in Section 3.3 we obtain the spectra shown in Figs. 6 and 7. The skew lineshapes of the main peak and plasmon satellites arise from the combined effect of quasiparticle recoil (which gives rise to lifetime broadening) and inelastic emission of bosonized low energy e–h pairs in the metal. The quasiparticle lifetime $\tau_{\mathbf{K}}$ is given by the FGR expression $\tau_{\mathbf{K}}^{-1} = 2\Gamma(\mathbf{K},\mathrm{IS}) = 2\pi\rho_2(\mathbf{K},\mathrm{IS},\omega=0)$. The relative peak intensities signify the regime of weak coupling to surface electronic excitations due to which $w_{\mathbf{K}} < 1$ and hence small spectral weight of the plasmon satellites. In Fig. 7 we also depict the threshold energy at which in the present weak coupling limit the GWA-based band bottom corrections should be implemented. Note that in the limit $\mathbf{K} \to 0$ such corrections are not needed because in that case the full spectrum appears as a convolution of the types given in expressions (26) and (49) which both exhibit correct threshold behaviour.

The features of the spectrum shown in Figs. 6 and 7, which reflect the weak coupling limit and $w_{\mathbf{K}} \ll 1$, are in contrast to the situation of photoexcited holes in bulk valence bands studied in Ref. [30] for which $w_{\mathbf{K}} \sim 1$. The latter situation with pronounced multiplasmon satellites could be retrieved

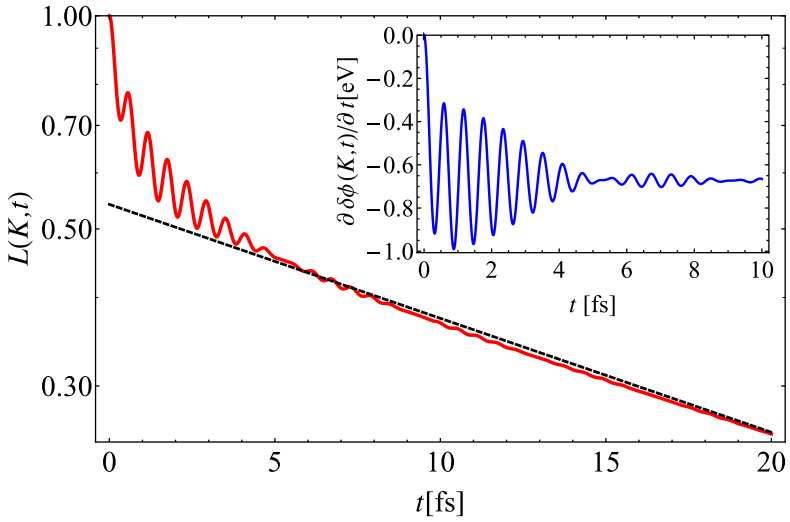

Fig. 9. Initial and preasymptotic behaviour of the survival probability $L(\mathbf{K},t)$ of an IS-electron characterized by the spectrum shown in Figs. 6 and 7 (note logarithmic scale on the vertical axis). Dashed line denotes the Markovian decay described by expression (52). Inset: Initial transient polarization shift of the IS-electron energy calculated using Eq. (36).

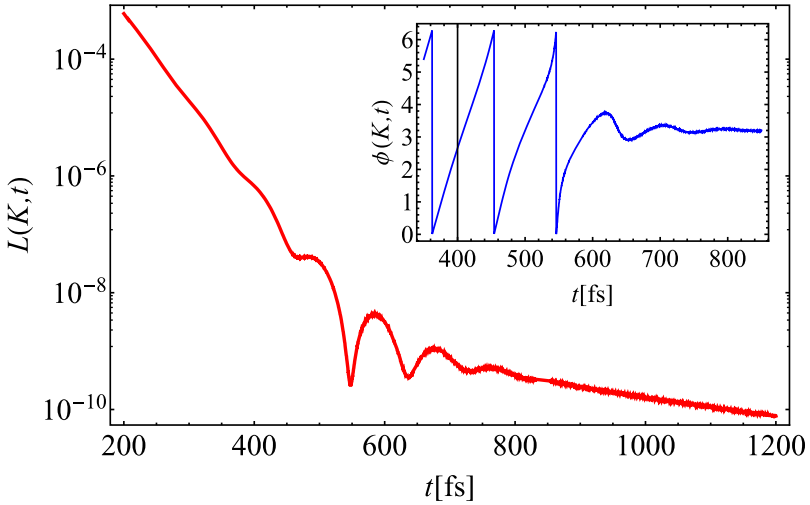

Fig. 10. Long time limit of the survival probability $L(\mathbf{K},t)$ from Fig. 9 with the transition from FGR to non-exponential asymptotic decay. The minimum attained for $t = 480$ fs signifies incomplete collapse of the quasiparticle amplitude. Inset shows the collapse of the quasiparticle phase (modulo 2π) in the same interval.

by rescaling the magnitude of the present model cumulant spectrum $\rho_2(\mathbf{K},\mathrm{IS},\omega)$ by a factor of 8. The spectrum resulting from such rescaled $\rho_2(\mathbf{K},\mathrm{IS},0)$ is illustrated in Fig. 8 and the comparison of peak intensities (after the time reversal) with those of the bulk hole spectra presented in Ref. [30] reconfirms that in image potential bands the coupling of quasiparticles to the charge density fluctuations is much weaker than in the bulk bands of the same substrate [69].

The quasiparticle survival probability $L(\mathbf{K}>0,t)$ calculated from the spectrum of Figs. 6 and 7 is shown in Figs. 9 and 10. The plots illustrate distinct stages of the dynamics of an electron promoted in a Q2D-band with initial $\mathbf{K}>0$. The early quasiparticle evolution within the Heisenberg uncertainty window is characterized by the transients during which the initial Zeno decay (22) is promptly succeeded by off-the-energy-shell processes dominated by excitation of virtual surface plasmons of energy $\omega_s \sim 7.5$ eV. This gives rise to the early beating of $L(\mathbf{K},t)$ with the period $\sim$0.5 femtosecond (fs) shown in Fig. 9. The attenuation of the beating and its dephasing (inset) originates from the width

of $\rho_2(\mathbf{K},IS,\omega)$ which is largely determined by the width of surface excitation spectrum $\mathcal{S}_{\mathrm{IS;IS}}(\mathbf{Q}, v)$ shown in Fig. 3, and to a lesser extent by the quasiparticle recoil energy $\epsilon_{\mathbf{K+Q}} - \epsilon_{\mathbf{K}}$. Past the ~7 fs long interval the energy conservation sets in and gives rise to a steady state quasiparticle decay due to the emission of real low energy e–h excitations in the solid. Here the real or on-shell plasmon excitations are not possible because $\epsilon_{\mathbf{K}} < \omega_s$. In this intermediate interval the decay of the initial state as described by (35) is Markovian. It follows exponential law governed by the FGR decay rate corrected (shifted) by the Debye–Waller exponent

$$L^{Mar}(\mathbf{K},t) = e^{-2[\Gamma(\mathbf{K},\mathrm{IS})t + w(\mathbf{K},\mathrm{IS})]}. \tag{52}$$

This limit is illustrated in Fig. 9 where its onset can be clearly pinpointed. The already available databases of calculated lifetimes refer to this intermediate regime of quasiparticle evolution [69].

The preasymptotic Markovian decay (52) cannot continue indefinitely because for yet longer times the presence of the band bottom in the spectrum gives rise to a contribution to the quasiparticle amplitude which causes a much slower asymptotic inverse power [58,70] or combined inverse power and logarithmic decay [25,20]. The crossover between the two types of decays is characterized by the interference of the FGR amplitude and the "return" amplitude oscillating with frequency of the order of the effective band width [70]. This interference causes a collapse of the survival probability which, depending on the quasiparticle spectral properties, may be either complete or incomplete. The onset of interference and crossover to asymptotic stage of quasiparticle evolution corresponding to the spectrum of Fig. 6 is illustrated in Fig. 10. This onset puts the upper temporal bound on the detection of standard quasiparticle energies and lifetimes because the identity of the initial quasiparticle state, contained in the amplitude and phase of (5), is lost beyond the collapse.

The ubiquitous early transients and late collapse which characterize quasiparticle dynamics in surface bands have several important ramifications. In particular, they restrict the applicability of standard optical Bloch equations (OBE) describing multilevel systems solely to the Markovian window in which (52) holds. This point will be further discussed in the next section.

Lastly, we comment on the role played by interband transitions in the modification of quasiparticle dynamics. According to (48), inclusion of additional scattering channels $n \to n'$ has a twofold effect on $\rho_2(\mathbf{K},n,\omega)$. First, it makes $\rho_2(\mathbf{K},n,\omega)$ nonvanishing down to the lowest unoccupied state(s) in the n'th bands and second, enhances it over the width of the nth band. This, in turn, eliminates the occurence of bound states below the nth band bottom, reduces the Zeno and FGR lifetimes, and shifts the onset of quasiparticle collapse to longer evolution times. The situation becomes more complicated for interband transitions to the states close to the Fermi energy in partly occupied bands. As noted earlier [33], the description of quasiparticle dynamics in terms of retarded single electron propagators (5) becomes inappropriate when the effects of interaction (3) must be included in the initial ground state $|0\rangle$ that incorporates partly occupied bands. In this case causal propagators with the corresponding self-energy expansion should be used instead of the retarded ones to yield the quasiparticle spectra [25].

5. Manifestations of nonadiabatic dynamics and decoherence in ultrafast experiments

Perturbations of the surface electronic structure by ultrafast probes bring the system into excited states with electrons and holes created in empty and occupied bands, respectively. The relaxation of these states proceeds on the time scales determined by the interactions of excited quasiparticles with the heatbath. In the case of metallic surfaces the promotion of electrons (holes) into empty (occupied) surface bands produces a nonequilibrium charge distribution which induces strong ultrafast response of the surrounding electron density. Quantum transients, decay and decoherence effects arising in response of the environment to creation of quasiparticles in excited states of the probed system that have been elaborated in Section 4 are designated the intrinsic effects [42]. They are expected to manifest themselves most clearly in the state-resolved measurements. The latter should be designed to yield spectral properties of the quasiparticles with high energy resolution or reveal their evolution on the ultrashort time scale. On the theoretical grounds, information on either spectral or temporal aspects of state-resolved quasiparticle dynamics is contained in the propagators which describe quasiparticle evolution during the various stages of ultrafast experiments. These propagators are the basic

constituents of higher order correlation functions describing the various spectroscopic measurements [1,5,6,9,10,13–15,22,31,32,41,44,45,49,53,62,88].

In the preceding sections we have presented a method for construction and calculation of the propagators of electrons excited into empty bands and holes created in occupied bands in which they are subject to the interactions with bosonic degrees of freedom that model the excitations of the system heatbath. This construction enables the studies of multiexcitation dynamics and complete quasiparticle spectral properties within a unified framework. The developed formalism should prove particularly useful in descriptions of the various manifestations of nonadiabatic hot electron and hole dynamics in surface bands which have come in the focus of many experimental and theoretical investigations with the advent of time-resolved spectroscopies.

Besides the lifetime effects, which have been the most studied manifestations of decay processes in surface bands [69], quantum transients and associated decoherence phenomena may strongly affect the state resolved measurements of quasiparticle dynamics during the early propagation intervals. Our analyses carried out in this and the preceding works [18–21,15,71] illustrate that the standard quasiparticle evolution in surface bands, that is conventionally characterized by exponential or FGR decay of the well defined initial quantum state, is established after the initial transients die out, about few femtoseconds upon the quasiparticle promotion into a band eigenstate. The evolution governed by exponential decay may proceed for several hundreds of femtoseconds before the interference effects give rise to the collapse of quasiparticle amplitude [58] and phase [20,21,15]. The interval between the establishment of the FGR-governed quasiparticle decay and its collapse is designated the quasiparticle lifespan. During this interval the motion of quasiparticles in surface bands can be characterized by the energies and lifetimes comprehensively reviewed in Ref. [69]. Outside this interval the quasiparticle propagation is overwhelmed by the early and late transients that completely destroy the standard quasiparticle features. These transients are true quantum–mechanical phenomena which have already been experimentally detected in the real time domain [47,48,61], albeit not yet in condensed matter systems for which their temporal manifestations have been only anticipated [18–21,77]. The following discussion describes experimental situations and regimes in which such intrinsic processes may produce experimentally detectable effects in spectroscopic studies of the surface electronic structure.

Typical examples of the steady-state spectroscopies of surface bands are the direct (1PPE) and inverse photoemission (IPE or BIS) spectroscopy which reveal the spectra of occupied and unoccupied electronic states, respectively. Since the electron and hole spectra are related by time reversal one can use the properties of quasiparticle propagators of the form (5) and their spectra shown in Figs. 9 and 10 to discuss the role of nonadiabatic surface response on the spectral shapes in both spectroscopies. For historical reasons we first briefly outline these effects in the 1PPE spectra from occupied levels at surfaces because the earliest direct evidence of transient phenomena has come from this spectroscopy. In this context particularly illustrative are the photoelectron spectra from occupied levels of adsorbates which due to their localization outside the substrate bulk region provide information on strictly surface localized electron dynamics. Transient and nonadiabatic effects lead to two major modifications of the spectral distributions of occupied surface localized states revealed by 1PPE spectroscopy. The first is a combined effect of asymmetric spread (skewing), upward polarization shift and Debye–Waller-factor scaling of the primarily lifetime broadened quasiparticle peak (in this case of the hole) for all states $|\mathbf{K}\rangle$ in the occupied bands of finite width, as well as for the localized orbitals and nonbonding levels broadened by lifetime effects only. The second is the occurrence of satellite structures below the main peak provided the hole coupling to the surface response is strong enough. The origin of such spectral features was analyzed and their manifestations in the early experiments reviewed in Sections 3 and 4 of Ref. [62]. These experiments provided strong evidence for multiexcitation processes in the studied systems. Currently attainable much higher resolution of 1PPE spectroscopy should enable new insights into these effects and the underlying ultrafast phenomena.

In contrast to 1PPE, in which an electron is removed from an occupied state of the system, in IPE an electron is added to the system in a radiative transition from an initial free particle state into a final band or bound state. Then, the energy distribution of emitted photons reveals the energy spectrum of the final electron state. Unoccupied adsorbate levels and image potential states on metal surfaces have been studied by this technique [78–83] and their broadening discussed in the context of the afore de-

scribed theory [84,85]. The signatures of multiexcitation processes involving soft substrate e–h pairs and interband relaxation may have been discerned whereas real surface plasmon excitations have not been observed, possibly due to poorly defined plasmons in the studied systems (noble and transition metals) and insufficient experimental resolution available in the early experiments. Novel performances of IPE might lead to more conclusive results but higher resolution achieved in 2PPE from surface bands have favoured the use of this spectroscopy over the IPE.

Although not truly state resolved, optical absorption measurements have proved as one of the most valuable tools in the investigations of electron band structure of various materials. Theoretical studies of the role of transient effects in the spectra of optically induced valence-to-conduction band transitions in metals and degenerate semiconductors have a long history and are commonly termed the Mahan–Nozières–De Dominicis (MND) problem [22]. Here the major difficulty arises in connection with an equivalent treatment of the excitonic interaction of the optically excited electron with the hole left behind (vertex corrections), on the one hand, and the separate interactions of the electron and hole with the charge density fluctuations in the solid (self-energy corrections), on the other hand, as well as their interference. Model calculations of these phenomena are based on finding the solution of Bethe–Salpeter equation (BSE) in the electron–hole scattering channel in which the vertex and self-energy corrections from multiexcitation processes must be treated on the same level of consistency and accuracy. Elegant and insightful solutions of the MND problem applicable to bulk systems exist only for simplified forms of the interparticle interactions, such as the screened static, contact or separable interparticle potentials (for details see Refs. [22,32,53]). All these solutions invariably predict observable many-body modifications of the threshold part of optical absorption spectra which arise from transient perturbations of the Fermi sea. Semiquantitative estimates of the transient and many-body induced spectral features have also been reported for optically induced transitions in adsorbates (see Section 5C in Ref. [62] and Section V in Ref. [85]). In the original formulation of the MND model the self-energy renormalizations of the excited electrons were absent because the model was designed to treat the optical absorption spectra at the excitation threshold that coincides with the Fermi level.

Later extensions and elaborations of the MND model to partly or fully account for the dynamical character of interparticle interactions were carried out in the GWA for self-energy and in the ladder approximation (LA) for vertex corrections [86–89] which satisfy the same level of selfconsistency in the BSE. Their applications to bulk absorption spectra show the expected partial cancellation (interference) of self-energy and vertex effects [90] and the occurrence of extra many-body induced spectral features already noted in exact solutions of the simple models [53]. Calculations of equivalent complexity have not yet been reported for metallic surfaces. However, it may be anticipated that the optical absorption spectra involving transitions from occupied to unoccupied surface bands may bear additional specificities relative to the analogous ones in the bulk. At metal surfaces the strong initial bare Coulomb interaction between the excited electron and hole (primary excitonic interaction) will be heavily screened on the femtosecond time scale by the surface electronic response [71]. This means that subsequent electron and hole motion will be dominantly governed by the individual interaction of each quasiparticle with its own screening (image) charge which develops simultaneously with the fading of primary e–h interaction. Therefore, the long time limit of optical absorption amplitude will to a good approximation be given by the **K**-momentum sum over the products of excited quasiparticle propagators of the form (5) for the electron and its hole counterpart. This implies that in the energy domain the optical absorption spectrum is given by the momentum sum over the convolutions of the excited electron spectra $\mathcal{N}(\mathbf{K}, \omega)$ defined in (7) with the analogously defined and calculated hole spectra. Hence, on the basis of the earlier [91,71] and present work it may be envisaged that the optical absorption spectra of surface bands should, in addition to the FGR-lifetime broadening of spectral lines, also bear the signatures of quantum transients and decoherence processes associated with the afore elaborated nonadiabatic dynamics of each quasiparticle alone.

Transient phase and amplitude variations of quasiparticles excited in the system, whose behaviour follows the patterns illustrated in Figs. 9 and 10, are expected to particularly affect the experiments sensitive to phase accumulations in sequential excitation and deexcitation processes, like in the transient m-wave mixing spectroscopies [1,92] (e.g. four wave mixing-FWM, Raman, etc.). For short delays between narrow excitation pulses the intermediate states of the system may be dominated by such "intrinsic" transients. This may have a strong effect on the coherence of final signal, in addition to

the effects arising from the modulation of excitation pulses. Here it is important to note that the necessity for a careful examination of ultrafast phenomena in FWM spectroscopy of complex systems was pointed out long ago in a very insightful review on phase and amplitude dynamics of coherent transients in semiconductor quantum wells [93].

In contrast to optical absorption measurements the time, energy and angular resolved two-photon (2PPE) or multi-photon photoemission (MPPE) spectroscopy of surface electronic structure probes the system that has already been excited by the pump pulse(s). Thereby pump–probe spectroscopies can provide the desired information on the dynamics of intermediate excited states partaking in the bound–unbound electron transitions that produce the final photoelectron yield. Here we shall discuss the implications of transient interactions and multiexcitation processes using the example of 2PPE from surface bands on metals [5,15].

In the first step of 2PPE from a surface state band (SS-band) the electron excited by the pump pulse and the hole left behind are initially bound by the bare Coulomb interaction in a transient surface exciton [71]. Subsequent onset of dynamical screening has a twofold effect on the primary exciton. While the bare e–h interaction is being reduced by surface screening each quasiparticle develops its own image charge [95]. Fading of the excitonic interaction and simultaneous formation of the image charges of quasiparticles transforms the strongly correlated e–h pair into an electron and a hole propagating with negligible correlation in unoccupied IS- and occupied SS-band, respectively. (Note in passing that such primary excitonic interactions are not an exclusive intermediate of the 2PPE but they also take place in optical spectroscopy, electron energy loss spectroscopy, appearance potential spectroscopy and partial yield photoelectron spectroscopy.) In the case in which after the second step of 2PPE the interaction of photoemitted electrons with surface excitations can be neglected, the amplitude of the final signal in a completed pump–probe experiment appears to a good approximation as a convolution of the surface state hole and the intermediate and final state electron propagators integrated over all the pump pulse, probe pulse and final observation times [15,49]. In the more complicated case of MPPE one should also carry out state summations and time integrations over all products of intermediate state propagators before the final integration over the observation times.

Depending on the delay between the ultrashort pump and probe pulses relative to the duration of screening of the primary excitonic potential, the final signal will measure the properties of either dominantly unrelaxed (excitonic) or prevailingly relaxed image potential band states partaking in the intermediate steps of 2PPE or MPPE. The stages of electron evolution in the already established states in IS-bands on Cu (1 1 1) are discussed in Section 4.2 and shown in Figs. 9 and 10. They illustrate the effects arising from the dominant decoherence mechanism on metal surfaces which is generally system specific [94]. By invoking the time reversal, temporal evolution of the SS-holes excited by the pump pulse can be obtained in a similar fashion [19] and combined with those of intermediate electrons to obtain the transients in the final 2PPE signal.

One of the major goals of state resolved pump–probe spectroscopies of surface bands has been the determination of energies and lifetimes of the band states. Obviously, in order to be able to detect energies and lifetimes of quasiparticles propagating in the quasistationary intermediate band states the delay time between the pump and probe pulses should exceed the duration of the early transients, on the one hand, but still be shorter than the collapse onset times beyond which the quasiparticle identity is lost, on the other hand. In other words, it should range within the overlap of the Markovian windows or the lifespans of hot electrons and holes. In the Markovian window the quasiparticle amplitude can be represented by a simple form [cf. Eq. (52)]

$$\psi^{Mar}_{\mathbf{K},n}(t) \sim \mathcal{Z}_{\mathbf{K},n} e^{\mp i(\tilde{\epsilon}_{\mathbf{K},n} \mp i\Gamma_{\mathbf{K},n})t}, \tag{53}$$

where n is the band index, $\mathcal{Z}_{\mathbf{K},n} = e^{-w_{\mathbf{K},n}}$ and $\mp$ stands for electrons and holes, respectively. The establishment of the quasiparticle evolution described by (53) permits the application of optical Bloch equations [96] (OBE) to the studies of electron and hole dynamics in surface bands and their effect on the photoemission spectra. To this end one needs to construct the so-called $\widehat{\mathbf{\Gamma}}$-matrix which together with the optical transition matrix elements represent the main input for the OBE. The most exploited model in applications of the OBE to descriptions of 2PPE spectra from surface bands has been based on a three-level system in which the occupied (e.g. SS-state), intermediate unoccupied (e.g. an

IS-state) and final state bands are represented by single levels with energies ϵ_{SS}, ϵ_{IS}, ϵ_f, and decay rates $\Gamma_{SS} > 0$, $\Gamma_{IS} > 0$, $\Gamma_f = 0$, respectively. In this paradigmatic case the mapping of (53) to the elements of the density matrix which appear as solutions of the OBE describing 2PPE are given by [15]

$$\widehat{\Gamma} = \begin{pmatrix} 0 & \frac{\Gamma_{SS}+\Gamma_{IS}}{2} & \frac{1}{2}\Gamma_{SS} \\ \frac{\Gamma_{SS}+\Gamma_{IS}}{2} & (\Gamma_{SS}+\Gamma_{IS}) & \frac{2\Gamma_{SS}+\Gamma_{IS}}{2} \\ \frac{1}{2}\Gamma_{SS} & \frac{2\Gamma_{SS}+\Gamma_{IS}}{2} & \Gamma_{SS} \end{pmatrix}. \tag{54}$$

It should be reiterated that the applicability of the OBE based on the stationary matrix $\widehat{\Gamma}$ of the form (54) or its multilevel generalizations is restricted to the descriptions of 2PPE spectra only during the overlap of Markovian timespans of excited quasiparticles.

In the opposite situations, in which the ultrafast measurements may have a small overlap with the Markovian windows of participating quasiparticles, quantum transients may dominate the experimental results. Observation of such manifestations of nonadiabatic dynamics poses a challenge in its own right because their detection either in the temporal or spectral domain would provide yet another confirmation of the fundamental principles of quantum mechanics. It is hoped that the present work may motivate endeavours in this direction.

Acknowledgments

This work was supported in part by the Ministry of Science, Education and Sports of the Republic of Croatia through the Research Project No. 035–0352828-2839.

Appendix A. Invertibility of Eqs. (8) and (18)

Here we demonstrate the invertibility of expressions (8) and (18) following Ref. [45]. Denoting by $\widetilde{C}(\mathbf{k},t)$ the expression defined by Eq. (8), in which $\rho(\mathbf{k},\omega)$ is given by Eq. (18) with the dummy integration variable τ, we get

$$\begin{aligned} \widetilde{C}(\mathbf{k},t\geqslant 0) &= \int_{-\infty}^{\infty} d\omega \tfrac{1-i\omega t-e^{-i\omega t}}{\omega^2} \int_{-\infty}^{\infty} \tfrac{d\tau}{2\pi} \ddot{C}(\mathbf{k},\tau) e^{i\omega\tau} \\ &= \int_{-\infty}^{\infty} \tfrac{d\tau}{2\pi} \ddot{C}(\mathbf{k},\tau) \left[\int_{-\infty}^{\infty} d\omega \tfrac{e^{i\omega\tau}}{\omega^2} - it \int_{-\infty}^{\infty} d\omega \tfrac{e^{i\omega\tau}}{\omega} - \int_{-\infty}^{\infty} d\omega \tfrac{e^{i\omega(\tau-t)}}{\omega^2} \right]. \end{aligned} \tag{A1}$$

Making use of the representations

$$\frac{1}{2\pi i} \int_{-\infty}^{\infty} d\omega \frac{e^{i\omega\tau}}{\omega - i0^+} = \theta(\tau), \tag{A2}$$

$$\frac{1}{2\pi} \int_{-\infty}^{\infty} d\omega \frac{e^{i\omega\tau}}{(\omega - i0^+)^2} = -\tau\theta(\tau) \tag{A3}$$

for the terms in the square bracket on the RHS of (A1) we find using the boundary conditions (12) and (13) and integration by parts:

$$\begin{aligned} \widetilde{C}(\mathbf{k},t) &= \int_{-\infty}^{\infty} d\tau \ddot{C}(\mathbf{k},\tau)[t\theta(\tau) - \tau\theta(\tau) + (\tau - t)\theta(\tau - t)] = t\dot{C}(\mathbf{k},t) - \int_0^t d\tau\tau\ddot{C}(\mathbf{k},\tau) \\ &= C(\mathbf{k},t). \end{aligned} \tag{A4}$$

This proves the invertibility of expressions (8) and (18), i.e. the equivalence of information on quasiparticle dynamics contained in the quasiparticle spectrum (7) and $\rho(\mathbf{k},\omega)$ determined from Eqs. (18) and (21).

Appendix B. Quasiparticle spectrum from expansion of cumulant representation

Here we comment on an alternative approach to the derivation of quasiparticle spectrum pursued in Ref. [37] and bring it in relation to the present one. In Ref. [37] the calculations were based on direct expansion of expression (5) in a power series, viz.

$$G^0_{\mathbf{k}}(t)\exp[C_2(\mathbf{k},t)] \simeq G^0_{\mathbf{k}}(t)\exp\left[C_2^{pol}(\mathbf{k},t)\right]\left(1+C_2^{sat}(\mathbf{k},t)+\cdots\right), \tag{B1}$$

in which only the first two terms from the round bracket on the RHS of (B1) were retained and the whole expression then Fourier transformed to yield the spectrum. Note that when $\exp[C_2(\mathbf{k},t)]$ is associated with $G^0_{\mathbf{k}}(t)$ the consistent approach is to express $\rho_2(\mathbf{k},\omega)$ in $C_2^{sat}(\mathbf{k},t)$ in terms of the relaxed energies $\tilde{\epsilon}$. The first spectral component arising from this procedure is the DWF-weighted δ-function for the quasiparticle peak

$$\mathcal{N}^{(0)}(\mathbf{k},\omega') = \left(1-\int\frac{\rho_2(\mathbf{k},\omega)}{\omega^2}d\omega\right)\delta(\omega'-\tilde{\epsilon}_{\mathbf{k}}). \tag{B2}$$

The spectral structure outside the range of (B2) reads

$$\mathcal{N}^{(1)}(\mathbf{k},\omega') = \frac{\rho_2(\mathbf{k},\omega'-\tilde{\epsilon}_{\mathbf{k}})}{(\omega'-\tilde{\epsilon}_{\mathbf{k}})^2}. \tag{B3}$$

For $\omega' < \tilde{\epsilon}_{\mathbf{k}}$ this expression describes the desired dominant contribution to the spectral density between the band bottom and quasielastic peak, likewise the GWA result (41) of which it is a limiting case for $\omega'-\tilde{\epsilon}_{\mathbf{k}} \gg \Gamma_{\mathbf{k}}$. Then, in view of Eqs. (41)–(45) the form of (B3) is consistent with zero width of the quasiparticle peak in (B2). In the opposite limit $\omega' > \tilde{\epsilon}_{\mathbf{k}}$ expression (B3) describes the first satellite structure arising from the single excitations in the system. Expressions equivalent to (B2) and (B3) are also obtained from the first iteration of Dyson equation for the quasiparticle propagator [36]. However, such a procedure based on expansion (B1) gives an incomplete description of the spectral shape of quasiparticle peak because separate integrations of the t-dependent terms in the integrand on the RHS of (8) omit the quasiparticle decay processes described by the on-shell decay rate $\Gamma_{\mathbf{k}}$ which broadens the relaxed quasiparticle peak. This missing feature is then introduced *a posteriori* by hand [37]. It should also be noted that this procedure is inadequate for the description of multiexcitation processes leading to the multiple satellite structures or IR-power law spectra of the type (26) and (32), respectively.

References

[1] S. Mukamel, Principles of Nonlinear Optical Spectroscopy, Oxford University Press, New York and Oxford, 1995 (Chapter 1).
[2] For applications of ultrafast spectroscopies in the studies of surfaces see: H. Zacharias (Ed.), Dynamics of Electron Transfer Processes at Surfaces, Prog. Surf. Sci. 82 (2007) 161–388.;
U. Bovensiepen, H. Petek, M. Wolf (Eds.), Dynamics at Solid State Surfaces and Interfaces, Current Developments, vol. I, Wiley-VCH, 2010.
[3] For a review of the experimental aspects of 2PPE spectroscopy see: H. Petek, S. Ogawa, Prog. Surf. Sci. 56 (1997) 239. and references therein.
[4] H. Ueba, Surf. Sci. 334 (1995) L719.
[5] For review of the theory of 2PPE spectroscopy of surfaces see: H. Ueba, B. Gumhalter, Prog. Surf. Sci. 82 (2007) 193. and references therein.
[6] For unified theoretical approach to multiphoton photoemission and sum-frequency-generation spectroscopy see: C. Timm, K.H. Bennemann, J. Phys. Condens. Matter 16 (2004) 661.
[7] A. Winkelmann, W.-Ch. Lin, Ch.-T. Chiang, F. Bisio, H. Petek, J. Kirschner, Phys. Rev. B 80 (2009) 155128.
[8] M. Schenk, M. Krüger, P. Hommelhoff, Phys. Rev. Lett. 105 (2010) 257601.
[9] I. Adawi, Phys. Rev. 134 (1964) A788.
[10] N.W. Ashcroft, W.L. Schaich, National Bureau of Standards Special Publication 323 (1970) 129.;
W.L. Schaich, N.W. Ashcroft, Phys. Rev. B 3 (1971) 2452.
[11] G.D. Mahan, Phys. Rev. B 2 (1970) 4334.
[12] D.C. Langreth, Phys. Rev. B 3 (1971) 3120.
[13] J.-J. Chang, D.C. Langreth, Phys. Rev. B 5 (1972) 3512;
J.-J. Chang, D.C. Langreth, Phys. Rev. B 8 (1973) 4638.
[14] C. Caroli, D. Lederer-Rozenblatt, B. Roulet, D. Saint-James, Phys. Rev. B 8 (1973) 4552.
[15] P. Lazić, D. Aumiler, B. Gumhalter, Surf. Sci. 603 (2009) 1571.

[16] D. Abramavicius, B. Palmieri, D.V. Voronine, F. Šanda, S. Mukamel, Chem. Rev. 109 (2009) 2350.
[17] B. Gumhalter, Phys. Rev. B 72 (2005) 165406.
[18] P. Lazić, V.M. Silkin, E.V. Chulkov, P.M. Echenique, B. Gumhalter, Phys. Rev. Lett. 97 (2006) 086801.
[19] P. Lazić, V.M. Silkin, E.V. Chulkov, P.M. Echenique, B. Gumhalter, Phys. Rev. B 76 (2007) 045420.
[20] B. Gumhalter, A. Šiber, H. Buljan, Th. Fauster, Phys. Rev. B 78 (2008) 155410.
[21] S. Marion, B. Gumhalter, Phys. Status Solidi B, in press, http://dx.doi.org/10.1002/pssb.201100543.
[22] G.D. Mahan, Many Particle Physics, Plenum Press, New York and London, 1981 (Chapters 6 and 7).
[23] B. Gerlach, H. Löwen, Rev. Mod. Phys. 63 (1991) 63. and references therein.
[24] U. Weiss, Quantum Dissipative Systems, World Scientific, Singapore, New Jersey, London, Hong Kong, 1999.
[25] S. Engelsberg, J.R. Schrieffer, Phys. Rev. 131 (1963) 993.
[26] L. Hedin, Phys. Rev. 139 (1965) A796.
[27] G.D. Mahan, Comments Condens Matter Phys. 16 (1994) 333.
[28] B.I. Lundqvist, Phys. Konden. Materie 6 (1967) 193;
L. Hedin, Phys. Scr. 21 (1980) 417.
[29] B. Holm, U. von Barth, Phys. Rev. B 57 (1998) 2108.
[30] F. Aryasetiawan, L. Hedin, K. Karlsson, Phys. Rev. Lett. 77 (1996) 2268. and references therein.
[31] C.-O. Almbladh, J. Phys. Conf. Ser. 35 (2006) 127. and references therein.
[32] J. Gavoret, P. Nozières, B. Roulet, M. Combescot, J. Phys. (Paris) 30 (1969) 987.
[33] S. Doniach, Phys. Rev. B 2 (1970) 3898.
[34] A.E. Ruckenstein, S. Schmitt-Rink, Phys. Rev. B 35 (1987) 7551.
[35] T. Uenoyama, L.J. Sham, Phys. Rev. Lett. 65 (1990) 1048.
[36] F. Bechstedt, Phys. Status Solidi B 112 (1982) 9 (Section 6).
[37] F. Bechstedt, M. Fiedler, C. Kress, R. Del Sole, Phys. Rev. B 49 (1994) 7357.
[38] R. Del Sole, L. Reining, R.W. Godby, Phys. Rev. B 49 (1994) 8024.
[39] E.L. Shirley, Phys. Rev. B 54 (1996) 7758.
[40] A. Schindlmayr, R.W. Godby, Phys. Rev. Lett. 80 (1998) 1702.
[41] D.C. Langreth, Phys. Rev. B 1 (1970) 471.
[42] D.C. Langreth, Nobel 24 (1973) 210.
[43] E. Müller-Hartmann, T.V. Ramakrishnan, G. Toulouse, Phys. Rev. B 3 (1971) 1102.
[44] C. Blomberg, B. Bergersen, Can. J. Phys. 50 (1972) 2286.
[45] C.-O. Almbladh, L. Hedin, in: E.E. Koch (Ed.), Handbook on Synchrotron Radiation, vol. 1, North-Holland, Amsterdam, 1983 (Chapter 8).
[46] C. Verdozzi, R.W. Godby, S. Holloway, Phys. Rev. Lett. 74 (1995) 2327.
[47] S.R. Wilkinson, C.F. Bharucha, M.C. Fischer, K.W. Madison, P.R. Morrow, Q. Niu, B. Sundaran, M.G. Raizen, Nature 387 (1997) 576.
[48] C. Rothe, S.I. Hintschich, A.P. Monkman, Phys. Rev. Lett. 96 (2006) 163601.
[49] M. Sakaue, J. Phys. Condens. Matter 17 (2005) S245.
[50] A. Šiber, B. Gumhalter, Phys. Rev. Lett. 90 (2003) 126103.
[51] S. Doniach, E.H. Sondheimer, Green's Functions for Solid State Physicists, WA Benjamin Inc., New York, 1974.
[52] R. Kubo, J. Phys. Soc. Jpn. 17 (1962) 1100.
[53] P. Nozières, C.T. De Dominicis, Phys. Rev. 178 (1969) 1097.
[54] D. Dunn, Can. J. Phys. 53 (1975) 321.
[55] O. Gunnarsson, V. Meden, K. Schönhammer, Phys. Rev. B 50 (1994) 10462.
[56] W. Brenig, B. Gumhalter, J. Phys. Chem. B 108 (2004) 14549.
[57] D.K. Sunko, B. Gumhalter, Am. J. Phys. 72 (2004) 231.
[58] L. Khalfin, Sov. Phys. JETP 6 (1958) 1053.
[59] A.A. Abrikosov, L.P. Gor'kov, I.Ye. Dzyaloshinski, Quantum Field Theoretical Methods in Statistical Physics, Pergamon Press, Oxford, 1965 (Chapter II).
[60] O.S. Barišić, Phys. Rev. B 69 (2004) 064302;
O.S. Barišić, Europhys. Lett. 77 (2007) 57004.
[61] P. Facchi, S. Pascazio, J. Phys. A Math. Theor. 41 (2008) 493001.
[62] B. Gumhalter, Progr. Surf. Sci 15/1 (1984) 1.
[63] Contrary to the popular belief these tails are generally not Lorentzian-like. The spectral wing shapes far away from the QE peak are determined by the short time behaviour of $\exp[C(\mathbf{k},t)]$ which due to (22) does not give rise to Lorentzian tails in the quasiparticle spectrum $\mathcal{N}(\mathbf{k},\omega')$.
[64] A similar procedure of remeding the threshold properties of multiple boson excitation probabilities was introduced in Section IV of Ref. [56].
[65] The mapping $\mathcal{N}(\omega') \rightarrow \rho(\omega)$ in which $\mathcal{N}(\omega')$ exhibits a sharp upper band edge cutoff may give rise to negative values of the cumulant spectrum $\rho(\omega)$ in certain intervals of ω, likewise in Section 3.2.2.
[66] The root giving the position of GWA plasmaron maximum exceeds $E_{\mathbf{k}}$ by more than the surface plasmon excitation energy [28].
[67] An analogous identification of the corresponding quantities was carried out in Ref. [30].
[68] E.V. Chulkov, V.M. Silkin, P.M. Echenique, Surf. Sci. 437 (1999) 330.
[69] For recent reviews on quasiparticle lifetimes in surface bands see P.M. Echenique, R. Berndt, E.V. Chulkov, Th. Fauster, A. Goldman, U. Höfer, Surf. Sci. Rep. 52 (2004) 219;
E.V. Chulkov, A.G. Borisov, J.P. Gauyacq, D. Sánchez-Portal, V.M. Silkin, V.P. Zhukov, P.M. Echenique, Chem. Rev. 106 (2006) 4160;
J.M. Pitarke, M.G. Vergnigory, J. Phys. Condens. Matter 20 (2008) 304207;
W.-D. Schöne, Prog. Surf. Sci. 82 (2007) 161.
[70] E. Rufeil Fiori, H.M. Pastawski, Chem. Phys. Lett. 420 (2006) 35. and references therein.

[71] B. Gumhalter, P. Lazić, N. Došlić, Phys. Status Solidi B 247 (2010) 1907.
[72] V.M. Silkin, A.K. Kazansky, E.V. Chulkov, P.M. Echenique, J. Phys. Condens. Matter 22 (2010) 304013.
[73] The need for a separate treatment of the case **K** = 0 was also pointed out in Refs. [[25,43]].
[74] The inclusion of the effects of nondispersive surface plasmons amounts to taking a convolution of the spectrum from Eq. (49) with the spectrum from Eq. (26).
[75] A. Liebsch, Electronic Excitations at Metal Surfaces, Plenum Press, New York and London, 1997. and references therein.
[76] A. Marini, G. Onida, R. Del Sole, Phys. Rev. Lett. 88 (2002) 016403.
[77] K. Hyeon-Deuk, O.V. Prezhdo, Nano Lett. 11 (2011) 1845.
[78] F.J. Himpsel, Th. Fauster, Phys. Rev. Lett. 49 (1982) 1583.
[79] J. Rogozik, H. Scheidt, V. Dose, K.C. Prince, A.M. Bradshaw, Surf. Sci. 145 (1984) L481.
[80] B. Reihl, K.H. Frank, Phys. Rev. B 31 (1985) 8282.
[81] D. Straub, F.J. Himpsel, Phys. Rev. B 33 (1986) 2256. and references therein.
[82] R.A. Bartynski, T. Gustafsson, Phys. Rev. B 33 (1986) 6588;
S. Yang, K. Garrison, R.A. Bartynski, Phys. Rev. B 43 (1991) 2025.
[83] E. Bertel, U. Bischler, Surf. Sci. 307–309 (1994) 947;
E. Bertel, Surf. Sci. 331–333 (1995) 1136.
[84] B. Gumhalter, Surf. Sci. 157 (1985) L355.
[85] B. Gumhalter, K. Wandelt, Ph. Avouris, Phys. Rev. B 37 (1988) 8048.
[86] M. Rohlfing, S. Louie, Phys. Rev. B 62 (2000) 4927.
[87] N.-P. Wang, M. Rohlfing, P. Krüger, J. Pollmann, Phys. Rev. B 67 (2003) 115111.
[88] A. Marini, R. Del Sole, Phys. Rev. Lett. 91 (2003) 176402.
[89] A. Marini, C. Hogan, M. Grüning, D. Varsano, Comp. Phys. Commun. 180 (2009) 1392.
[90] F. Bechstedt, K. Tenelsen, B. Adolph, R. Del Sole, Phys. Rev. Lett. 78 (1997) 1528.
[91] W.-D. Schöne, W. Ekardt, Phys. Rev. B 62 (2000) 13464.
[92] Y.R. Shen, The Principles of Nonlinear Optics, Wiley-Interscience, Hoboken, New Jersey, 2003 (Chapters 14, 15 and 21).
[93] D.S. Chemla, J.Y. Bigot, Chem. Phys. 210 (1996) 135.
[94] For example of another type interactions and time scales of transients see Refs. [20,21].
[95] For the time scales of formation of image potential and corresponding bands see Figs. 5 and 6 in Ref. [71].
[96] For general reference see: C. Cohen-Tannoudji, J. Dupont-Roc, G. Grynberg, Atom–Photon Interactions, J. Wiley & Sons Inc., New York, 1992 (Chapter V).